DIAGNOSING CIRCUMSTELLAR DEBRIS DISKS

JOSEPH M. HAHN

Space Science Institute, 10500 Loring Drive, Austin, TX 78750, USA; jhahn@spacescience.org

ABSTRACT

A numerical model of a circumstellar debris disk is developed and applied to observations of the circumstellar dust orbiting β Pictoris. The model accounts for the rates at which dust is produced by collisions among unseen planetesimals, and the rate at which dust grains are destroyed due to collisions. The model also accounts for the effects of radiation pressure, which is the dominant perturbation on the disk's smaller but abundant dust grains. Solving the resulting system of rate equations then provides the dust abundances versus grain size and dust abundances over time. Those solutions also provide the dust grains' collisional lifetime versus grain size, and the debris disk's optical depth and surface brightness versus distance from the star. Comparison to observations then yields estimates of the unseen planetesimal disk's radius, and the rate at which the disk sheds mass due to planetesimal grinding. The model can also be used to measure or else constrain the dust grain's physical and optical properties, such as the dust grains' strength, their light-scattering asymmetry parameter, and the grains' efficiency of light scattering Q_s. The model is then applied to optical observations of the edge-on dust disk orbiting β Pictoris, and good agreement is achieved when the unseen planetesimal disk is broad, with $75 \lesssim r \lesssim 150$ AU. If it is assumed that the dust grains are bright like Saturn's icy rings ($Q_s = 0.7$), then the cross section of dust in the disk is $A_d \simeq 2 \times 10^{20}$ km^2 and its mass is $M_d \simeq 11$ lunar masses. In this case, the planetesimal disk's dust-production rate is quite heavy, $\dot{M}_d \sim 9\, M_\oplus$ Myr^{-1}, implying that there is or was a substantial amount of planetesimal mass there, at least 110 Earth masses. If the dust grains are darker than assumed, then the planetesimal disk's mass-loss rate and its total mass are heavier. In fact, the apparent dearth of any major planets in this region, plus the planetesimal disk's heavy mass-loss rate, suggests that the $75 \lesssim r < 150$ AU zone at β Pic might be a region of planetesimal destruction, rather than a site of ongoing planet formation.

Key words: protoplanetary disks – zodiacal dust

1. INTRODUCTION

A debris disk is a dusty circumstellar disk that is often found in orbit about a young star. It is also suspected that these dust disks might be sites of ongoing planet formation. This thinking is motivated by the dust grains' lifetime due to collisions, which is often much shorter than the age of the host star. Evidently, a circumstellar debris disk is also being supplied with fresh dust, and collisions among unseen planetesimals provide a plausible explanation for this dust production. Because planetesimals are also the seeds of planets, it is conceivable that a debris disk might be forming planets as well.

One should keep in mind that if the collisional grinding in the planetesimal disk is too vigorous, then it is possible that the planetesimals might instead grind away before they have a chance to assemble into planets. Indeed, models of the early evolution of the outer solar system propose that the early Kuiper Belt, which is a swarm of comets orbiting beyond Neptune, was initially composed of $M_{\rm KB} \sim 30$ Earth masses[1] (Kenyon 2002), which would be enough to allow for the formation of two Neptune-class planets, but that model also shows that runaway accretion during the next $t \sim 500$ Myr only managed to produce a handful of Pluto-sized bodies, while the bulk of the planetesimal mass there remained locked in the smaller planetesimals. Meanwhile, collisions among the smaller bodies steadily ground much of that mass to dust that is then blown out of the system by radiation pressure, which also stalls further growth. The mass-loss rate implied by this collisional grinding is $\dot{M}_d \sim t/M_{\rm KB} \sim 10^{13}$ gm s^{-1} (Stern & Colwell 1997; Kenyon 2002). Another outer solar system scenario is

the Nice model, which requires its primordial Kuiper Belt to persist until $t \sim 700$ Myr since formation, which is when the giant planets suddenly adjust their orbits and trigger the Late Heavy Bombardment (Gomes et al. 2005; Levison et al. 2008). Although the dynamical history of the Nice model is rather different from other models, it should be noted that this and most other models of the outer solar system's early evolution predict that the primordial Kuiper Belt had a quiescent period lasting several hundreds of millions years, during which the Belt would have lost tens of Earth masses of material due to collisional grinding and blowout of dust due to radiation pressure (Stern & Colwell 1997; Kenyon 2002).

An interesting question is whether the observed circumstellar debris disks have mass-loss rates comparable to that predicted for our early solar system. The answer to that question will then provide some guidance as to whether these disks should instead be thought of potential sites for planet formation, or else regions of planetesimal destruction. To address this issue, the following develops a model that follows the time evolution of a circumstellar debris disk. Sections 2.1–2.4 derive in some detail the model's physics, but readers not interested in those details can skip those sections. Sections 2.4.3–2.4.6 examine how the debris disk's structure and appearance depends upon the system parameters, and those results can also be quickly gleaned by inspecting the figures there. Section 3 then applies the model to observations of the debris disk orbiting β Pictoris, with Section 4 providing a summary of the findings.

2. THE DEBRIS-DISK MODEL

Radiation pressure is the dominate perturbation on small dust grains orbiting in a circumstellar debris disk (cf. Strubbe & Chiang 2006), and the review in Section 2.1 shows how the resulting dust orbits are simple functions of grain size. Dust

---

[1] The Kenyon (2002) model recommends 10 Earth masses in a 6 AU wide annulus centered at $r = 35$ AU, but this should be multiplied by $\sim$3 to account for the Kuiper Belt's full radial width.

collision rates are derived in Sections 2.2–2.3, and Section 2.4 shows how to use those rates to calculate the time evolution of the debris disk's dust abundance. The remaining subsections then illustrate how the simulated debris disk varies with the model parameters.

2.1. Dust Orbit Elements

An orbiting dust grain is characterized by its size parameter β, which is the ratio of stellar radiation pressure to gravity. For a spherical grain of radius R, the size parameter is

$$\beta = \frac{3L_\star Q_{rp}}{16\pi G M_\star c\rho R} = 0.57 Q_{\rm rp} \left(\frac{L_\star}{L_\odot}\right)\left(\frac{M_\star}{M_\odot}\right)^{-1}$$
$$\times \left(\frac{\rho}{1\ {\rm gm\ cm}^{-3}}\right)^{-1}\left(\frac{R}{1\ \mu{\rm m}}\right)^{-1}, \tag{1}$$

where $L_\star$ and $M_\star$ are the star's luminosity and mass, G is the gravitational constant, c is the speed of light, ρ is the grain's volume density, and $L_\odot$ and $M_\odot$ refer to solar values (Burns et al. 1979). The grain's radiation pressure efficiency is $Q_{\rm rp} = Q_a + (1 - g)Q_s$ (Burns et al. 1979), where Q_a is the efficiency of the grain's absorption of starlight and Q_s is the efficiency of light scattering by the grain. The scattering asymmetry parameter g is

$$g = \int \Phi(\phi) \cos\phi\, d\Omega, \tag{2}$$

where the integral runs over all solid angles, and the phase function $\Phi(\phi)$ gives the proportion of light that is scattered through scattering angle ϕ, which is the angle between the directions followed by the incident and scattered light. The phase function is normalized such that $\int \Phi(\phi)d\Omega = 1$, so $|g| \leqslant 1$. Forward scattering dust grains have values of $g > 0$, backscattering grains have $g < 0$, and isotropic light scattering has $g = 0$. The model developed here will be applied to the β Pictoris debris disk, whose dust grains are substantially larger than the wavelength of the incident light. This is the geometric optics limit, and energy conservation in this limit requires $Q_a + Q_s = 1$, so

$$Q_{\rm rp} = 1 - g Q_s. \tag{3}$$

Evidently, $Q_{\rm rp} \simeq 1$ except when $|g Q_s|$ is not small, which can occur if the dust grains are efficient forward or back scatters. Equation (1) shows that radiation pressure is significant for grains of radii $R \sim \mathcal{O}(1)\ \mu$m when orbiting a solar-type star, and is unimportant for grains with $R \gg 1\ \mu$m. Since radiation pressure has the same inverse-square force law as stellar gravity, the effects of radiation pressure are easily accounted for by substituting $GM_\star \to (1-\beta)GM_\star$ into all equations for the dust grains' motion.

Dust is manufactured when planetesimals collide. Consider a dust grain that is generated by colliding planetesimals that reside in nearly circular orbits of radius r. These planetesimals have a specific energy $E_p =$ kinetic + potential energy that is

$$E_p = \frac{1}{2}v^2 - \frac{GM_\star}{r} = -\frac{GM_\star}{2r}, \tag{4}$$

where $v = \sqrt{GM_\star/r}$ is the planetesimal's velocity, assuming its orbit is circular or nearly so. However, a dust grain that forms via a collision at radius r will have a specific energy

$E_d = \frac{1}{2}v^2 - GM_\star(1 - \beta)/r = -GM_\star(1 - \beta)/2a$, where a is the dust grain's semimajor axis. This assumes that the dust grain has the same velocity v as its parent planetesimal at the moment of its creation, or equivalently, the velocity at which the grain is ejected from the planetesimal is small compared to its orbital speed. But this is reasonable since the debris disks considered here are thin, which implies that dust generation occurs with low ejection speeds. In this case, $\frac{1}{2}v^2 = GM_\star/2r$ in the above, so the dust grain's semimajor axis is (Thébault et al. 2003)

$$a(\beta) = \frac{1 - \beta}{1-2\beta}r. \tag{5}$$

Bound orbits have $a > 0$, so only dust having $\beta < \beta_{\max}$ where $\beta_{\max} = \frac{1}{2}$ will populate the resulting debris disk, while dust having $\beta \geqslant \beta_{\max}$ are not bound to the star and quickly leave the system. According to Equation (1), the smallest bound grains have radii

$$R_{\min} = \frac{3L_\star Q_{\rm rp}}{16\pi\beta_{\max}GM_\star c\rho}$$
$$= 1.1 Q_{\rm rp}\left(\frac{L_\star}{L_\odot}\right)\left(\frac{M_\star}{M_\odot}\right)^{-1}\left(\frac{\rho}{1\ {\rm gm\ cm}^{-3}}\right)^{-1}\mu{\rm m}. \tag{6}$$

Next, note that a planetesimal's specific angular momentum $L_p = rv$ also equals the dust grain's angular momentum L_d, since both have the same position and velocity at the moment of the grain's creation. Since a dust grain's Keplerian orbit has $L_d = \sqrt{GM_\star(1 - \beta)a(1 - e^2)}$ while the planetesimal's $L_p = \sqrt{GM_\star r} = L_d$, this provides the grain's eccentricity

$$e(\beta) = \frac{\beta}{1 - \beta} \tag{7}$$

(Thébault et al. 2003). The dust grain's periapse $q_{\rm peri}$ and apoapse $Q_{\rm apo}$ distances are then

$$q_{\rm peri} = a(1 - e) = r \tag{8a}$$

$$\text{and}\quad Q_{\rm apo} = a(1 + e) = r/(1-2\beta), \tag{8b}$$

where r is the orbital radii of the planetesimals that gave birth to the dust. Also note that periapse is precisely at the planetesimal's orbit, which tells us that the grain's longitude of periapse $\tilde\omega$ is also the longitude where the grain formed.

2.2. Streamlines

Assessing the collisions that a dust grain experiences over its lifetime can be a laborious calculation, one that usually requires evaluating integrals over the dust grains' size distribution and the debris disk's three-dimensional volume. However, those integrals can be replaced by a simple summation when the model disk is quantized (see, for example, Krivov et al. 2006). In the following, the planetesimal disk, which is the source of this dust, is represented by N_r concentric rings that have radii r uniformly distributed over the interval $r_{\rm in} \leqslant r \leqslant r_{\rm out}$. Each planetesimal ring also produces dust at N_l discreet sites that are distributed uniformly in longitude about the ring. The dust grains' radii $R = (\beta_{\max}/\beta)R_{\min}$ are also quantized so that they uniformly sample the interval $R_{\min} < R < R_{\max}$, with N_β size bins in the interval $0 < \beta < \beta_{\max}$. As a result, the planetesimal

disk produces dust whose grains inhabit $N_s = N_r N_l N_\beta$ distinct streamlines, or orbits, whose shapes are given by Equations (5) and (7), and whose orientations are uniformly distributed in longitude.

The rate of dust production $p(R, r)$ by the planetesimal disk is also a power law, with $p(R, r) \propto R^{-q}$ being the rate at which the planetesimals inject dust of radii R into a single streamline, with q being the power law for the grains' differential size distribution. The model will also allow for the dust-production rate to vary with the source planetesimals' radial distance r as $p(R, r) \propto (r/r_{out})^c$. A planetesimal disk having $c < 0$ can then be thought of as experiencing "inside-out" erosion, since the inner portion of that disk experiences greater dust production than its outer parts, while a disk having $c > 0$ suffers "outside-in" erosion. Also note that $R \propto \beta^{-1}$, so the dust-production rate can be written $p(\beta, r) = p_0(\beta/\beta_{max})^q(r/r_{out})^c$ where p_0 is a constant.

Since there are $N_s = N_r N_l N_\beta$ streamlines in the model debris disk, the index i will be used to identify any one such dusty streamline, where $1 \leqslant i \leqslant N_s$. The streamlines' longitudes of periapse $\tilde{\omega}_i$ are uniformly distributed such that the resulting debris disk has N_l-fold symmetry. The quantity $n_i(t)$ will be the number of dust grains inhabiting streamline i at time t; these grains all have the same size β_i and orbit elements $a_i, e_i, \tilde{\omega}_i$, and they all formed at the same longitude $\tilde{\omega}_i$ in the same planetesimal ring that has radius r_i. The streamline's abundance $n_i(t)$ will then evolve over time t due to the production of dust by the planetesimal ring r_i, but that quantity will also vary due to collisions with the dust grains that inhabit the disk's other streamlines. The rate at which these dust grains collide and destroy each other is derived below.

2.3. Collision Rates

Figure 1 shows a dust grain in streamline i as it crosses streamline j. The dust in these streamlines have radii R_i and R_j and velocities $\mathbf{v}_i$ and $\mathbf{v}_j$. Suppose for now that the debris disk is flat, and that all dust grains have zero inclinations. In this case, grain i would sweep across a length $\Delta\ell = 2(R_i + R_j)/\sin\phi_{ijk}$ in streamline j, where ϕ_{ijk} is the angle between vectors $\mathbf{v}_i$ and $\mathbf{v}_j$, so $\sin\phi_{ijk} = |\mathbf{v}_i \times \mathbf{v}_j|/v_i v_j$. This quantity depends not just on the streamlines' orbit elements a_i, e_i and a_j, e_j, but also on the streamlines' relative longitude of periapse $\tilde{\omega}_k = \tilde{\omega}_j - \tilde{\omega}_i$, which is why the k subscript is also introduced.

The linear density of dust grains in streamline j is λ_j, so particle i will collide with $\lambda_j \Delta\ell$ particles as it traverses streamline j. The flux of dust in this streamline is $\lambda_j v_j$, which is the rate at which grains cross a point in that streamline, so $\lambda_j v_j = n_j/T_j$ where n_j is the total number of grains in that streamline and $T_j = 2\pi\sqrt{a_j^3/(1 - \beta_j)GM_\star}$ is that streamline's orbit period. So the number of collisions that grain i suffers as it crosses this site in streamline j is $\Delta n_{ijk} = \lambda_j \Delta\ell = 2(R_i + R_j)n_j f_z/\sin\phi_{ijk} v_j T_j$, where the factor f_z is now introduced to account for the dust disk's vertical thickness. Note that f_z would be unity if streamlines in the dust disk were coplanar. However, a real disk has a vertical half-width $h = I r_{ijk}$, where I is the grains' characteristic inclination and r_{ijk} is the radial distance from the star where streamlines i and j cross, with the k subscript again indicating that that quantity also depends on the streamlines' relative longitude of periapse $\tilde{\omega}_k$. Thus $f_z = 2f_c(R_i + R_j)/2h = f_c(R_i + R_j)/I r_{ijk}$ is the probability that two grains in streamlines i and j are close enough in the vertical direction to come in contact, and the
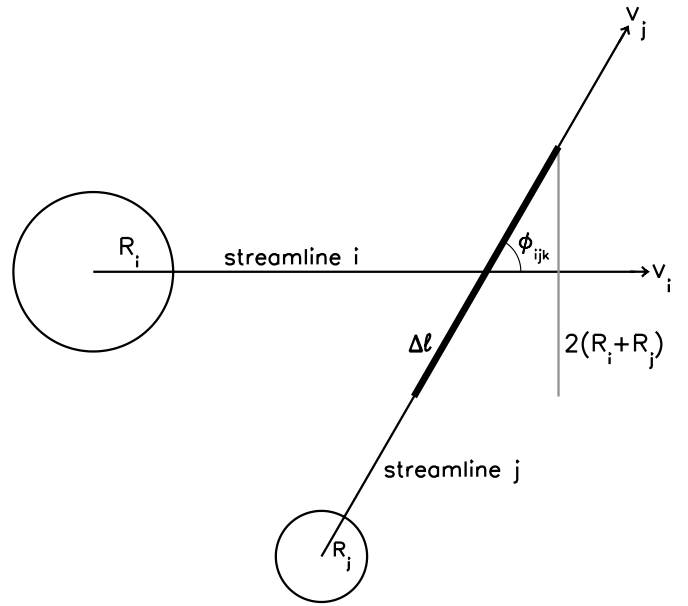
Figure 1. Dust grain of radius R_i crosses streamline j that contains dust of radii R_j. Grain i sweeps a length $\Delta\ell = 2(R_i + R_j)/\sin\phi_{ijk}$ along streamline j where $\sin\phi_{ijk}$ is the angle between the grains' velocity vectors $\mathbf{v}_i$ and $\mathbf{v}_j$.

factor $f_c = \pi/4$ is a geometric correction that accounts for the grain's circular cross section. Since there are n_i grains in streamline i, they will suffer $n_i \Delta n_{ijk}$ collisions with streamline j after one orbit period T_i, so the grains in streamline i collide with the grains in streamline j at site r_{ijk} at the rate $n_i \Delta n_{ijk}/T_i$. Thus, the total rate at which grains in streamline i suffer collisions with all of the disk's other streamlines is

$$\mathcal{R}_i = \sum \frac{n_i \Delta n_{ijk}}{T_i} = \frac{n_i}{T_{out}} \sum_{j=1}^{N_r N_\beta} \sum_{k=1}^{N_l} \sum_{r_1}^{r_2} \alpha_{ijk} n_j, \qquad (9)$$

where the coefficient $\alpha_{ijk} = \pi(R_i + R_j)^2 T_{out} f_{ijk}^c/2I \sin\phi_{ijk} r_{ijk} v_j T_i T_j$, and $T_{out} = 2\pi\sqrt{r_{out}^3/GM_\star}$ is the orbit period of the outermost planetesimal ring at $r = r_{out}$. Note that an additional factor f_{ijk}^c was also introduced into the above; it takes values of $f_{ijk}^c = 1$ if the collision with the impacting grain R_j is energetic enough to disrupt the target grain R_i, and with $f_{ijk}^c = 0$ if the collision does not disrupt grain R_i. The threshold for collisional disruption is given later in Section 2.3.2.

The leftmost sum in the above runs over streamlines that are composed of dust of radii R_j that have size parameters $\beta_j = \beta_{max}(R_{min}/R_j)$ produced by the planetesimal ring that has radius r_j; their orbit elements a_j and e_j are given by Equations (5) and (7). These dust grains have N_β possible sizes, and there are N_r such planetesimal rings, so $1 \leqslant j \leqslant N_\beta N_r$. The middle sum then accounts for the N_l sites in each planetesimal ring that produce dust having relative longitudes $\tilde{\omega}_k = \tilde{\omega}_j - \tilde{\omega}_i$, so $1 \leqslant k \leqslant N_l$. Also keep in mind that pairs of orbits cross at two sites $r_{ijk} = r_1$ and $r_{ijk} = r_2$ whose contributions are accounted for by the rightmost sum.

First we comment on differently sized dust grains that are produced at the same site within the same planetesimal ring. Such grains have the same longitude of periapse, $\tilde{\omega}_i = \tilde{\omega}_j$, and thus will re-encounter each other at periapse with the same velocity $\mathbf{v}_i = \mathbf{v}_j$. This also makes $\sin\phi_{ijk} = 0$, which might appear problematic because the collision probability α_{ijk} would seem to be singular there, but keep in mind that grains i and

j have the same velocity at periapse, namely, the planetesimal ring's velocity. Consequently, these grains have zero relative velocity at this particular site, so there is no chance for collisional fragmentation, and α_{ijk} is set to zero in this instance.

A dust grain's velocity is $v_j = (2\pi r_{out}/T_{out})\sqrt{(1 - \beta_j)(2r_{out}/r_{ijk} - r_{out}/a_j)}$ where r_{ijk} is the distance from the star where streamlines i and j cross. Since $T_i/T_{out} = (a_i/r_{out})^{3/2}/\sqrt{1 - \beta_i}$, the α_{ijk} in the above then becomes

$$\alpha_{ijk} = \frac{\beta_{max}^2 f_{ijk}^c}{4I \sin\phi_{ijk}} \sqrt{\frac{1 - \beta_i}{2a_j/r_{ijk} - 1}} \left(\frac{\beta_i + \beta_j}{\beta_i\beta_j}\right)^2$$
$$\times \left(\frac{r_{out}^2}{r_{ijk}a_j}\right)\left(\frac{r_{out}}{a_i}\right)^{3/2}\left(\frac{R_{min}}{r_{out}}\right)^2. \quad (10)$$

This quantity is the collision probability density, in the sense that $\alpha_{ijk}n_j$ is the probability per time T_{out} that a dust grain in streamline i suffers a collision with the dust in streamline j at site r_{ijk}.

2.3.1. Orbit Crossing Sites

The r_{ijk} in Equation (10) is one of two sites where orbit i crosses orbit j, and it is sensitive to the orbits' relative longitude of periapse $\tilde{\omega}_k = \tilde{\omega}_j - \tilde{\omega}_i$. To solve for r_{ijk}, rotate the coordinate system so that the $\hat{x}$-axis points to orbit i's periapse. Requiring the two orbital ellipses to intersect yields

$$r_{ijk} = \frac{p_i}{1 + e_i \cos\theta} = \frac{p_j}{1 + e_j \cos(\theta - \tilde{\omega}_k)}, \quad (11)$$

where $p_i = a_i(1 - e_i)$ is the orbit's semilatus rectum and θ is measured from the $\hat{x}$ direction. Using $\cos(\theta - \tilde{\omega}_k) = \cos\theta \cos\tilde{\omega}_k + \sin\theta \sin\tilde{\omega}_k$ allows Equation (11) to be written as $A\cos\theta - B\sin\theta + C = 0$, where $A = e_i - pe_j\cos\tilde{\omega}_k$, $B = pe_j \sin\tilde{\omega}_k$, $C = 1 - p$, and $p = p_i/p_j$. Solving for $\sin\theta^2 = 1 - \cos\theta^2$ then yields $\cos\theta^2 + 2D\cos\theta + E = 0$ where $D = AC/(A^2 + B^2)$ and $E = (C^2 - B^2)/(A^2 + B^2)$, which has the solution

$$\cos\theta = -D \pm \sqrt{D^2 - E} \quad (12a)$$

$$\text{and} \quad \sin\theta = (A\cos\theta + C)/B. \quad (12b)$$

Solve Equations (12) for the two θ's and insert those into $r_{ijk} = p_i/(1 + e_i\cos\theta)$ to get the radial distances for where these orbits cross. Then rotate the coordinate system back, $\theta \to \theta + \tilde{\omega}_i$, to get the longitudes where these orbits cross. Note that Equations (12) are real when $D^2 \geqslant E$, which is the requirement for orbits i and j to cross.

To evaluate the $\sin\phi_{ijk}$ in Equation (10), the dust grain's radial velocity $v_{i,r}$ and tangential velocity $v_{i,\theta}$ need to be evaluated at the collision site. Those velocity components are

$$v_{i,r} = \frac{e_i a_i \Omega_i}{\sqrt{1 - e_i^2}} \sin(\theta - \tilde{\omega}_i) \quad (13a)$$

$$\text{and} \quad v_{i,\theta} = \frac{a_i\Omega_i}{\sqrt{1 - e_i^2}}[1 + e_i\cos(\theta - \tilde{\omega}_i)], \quad (13b)$$

where $\Omega_i = 2\pi/T_i$ is the grains' mean motion. These velocity components are then used to obtain $\sin\phi_{ijk} = |\mathbf{v}_i \times \mathbf{v}_j|/v_i v_j = |v_{i,r}v_{j,\theta} - v_{i,\theta}v_{j,r}|/v_i v_j$ where v_i is the grain's total velocity.

Note that the above ignored the grain's small vertical velocity $v_{i,z}$, which is of order $I v_i$. This is appropriate since $I \ll 1$. However, the following section will still need an estimate of the dust grains' relative velocity in the vertical direction when determining whether collisions are destructive. And since the model being developed here does not faithfully follow the dust grains' vertical motions, it is assumed here that any two pairs of dust grains have a relative vertical speed that is equal to their rms value, $|v_{i,z} - v_{j,z}| = \sqrt{(I v_i)^2 + (I v_j)^2}$.

2.3.2. Disruption Threshold

Now derive the threshold for a dust grain's collisional disruption. The target dust grain has mass m_i and velocity $\mathbf{v}_i$, and it is struck by an impacting dust grain of mass m_j and velocity $\mathbf{v}_j$. The two dust grains' relative velocity just prior to impact is $\mathbf{v}_r = \mathbf{v}_j - \mathbf{v}_i$, and the specific work that the impactor must do on the target grain in order to disrupt it is $Q^\star$. For simplicity, assume that any debris produced by the disruption of the target grain has zero dispersion velocity, which then provides the minimum energy that is needed for disruption. In the target dust grain's rest frame, the system's kinetic energy is $\frac{1}{2}m_j v_r^2$ just prior to impact. It is shown below that most collisions will shatter both the target and the impactor, so the post-impact debris will have a total energy $E = \frac{1}{2}m_j v_r^2 - Q^\star(m_i + m_j)$ where $Q^\star m_i$ is the work that must be done in order to shatter grain m_i. But this energy can also be written as $E = \frac{1}{2}m_i v_i'^2 + \frac{1}{2}m_j v_j'^2$ where v_i' is the post-impact speed of the debris from grain m_i, and v_j' is the post-impact speed of mass m_j in this reference frame. Momentum conservation also requires that $m_j v_r = m_i v_i' + m_j v_j'$. Solving the energy and momentum equations simultaneously then provides the post-impact speed of debris m_i,

$$v_i' = \frac{m_j v_r}{m_i + m_j}\left[1 + \sqrt{1 - \frac{2(m_i + m_j)^2 Q^\star}{m_i m_j v_r^2}}\right]. \quad (14)$$

Keep in mind that this is the speed of debris in the reference frame where mass m_i was stationary just before impact. Consequently, the speed of that debris in the inertial reference frame is

$$\mathbf{v}_i + v_i'\hat{\mathbf{v}}_r, \quad (15)$$

where $\hat{\mathbf{v}}_r$ is the unit vector that points in the direction of $\mathbf{v}_r$.

The collision is energetic enough to disrupt grain m_i when Equation (14) is real, which requires $v_r^2 \geqslant 2(m_i + m_j)^2 Q^\star/m_i m_j$. Assuming all grains are spheres of similar density, this requirement becomes

$$v_r^2 > \frac{2Q^\star\left(\beta_i^3 + \beta_j^3\right)^2}{(\beta_i\beta_j)^3}. \quad (16)$$

When the above is satisfied, the collision is fast enough to destroy the target grain β_i, which is accounted for in Equation (10) by setting $f_{ijk}^c = 1$, while $f_{ijk}^c = 0$ when the above is not satisfied. In that case grain m_i will recoil from the collision and enter a new orbit about the star. However, nearly all collisions result in the disruption of grain m_i, so it is safe to ignore these rare non-disruptive collision events.

Unfortunately, the dust grains' collisional specific energy $Q^\star$ is rather uncertain, and likely depends on the target grain's size R_i (Holsapple et al. 2002). Another difficulty is that experimental measurements of $Q^\star$ only extend down to centimeter-sized targets (Holsapple 1994). However, models of observed debris

disks suggest $Q^\star \sim 3 \times 10^6$ erg gm^{-1} (Wyatt et al. 2007b), while Strubbe & Chiang (2006) recommend a nominal value of $Q^\star \sim 10^7$ erg gm^{-1} if the dust grains are rocky. But if circumstellar dust grains are icy, then values $\sim$100 smaller are possible (Holsapple et al. 2002). Strubbe & Chiang (2006) also note that sandblasting machines accelerate destructive particles to $v \sim 100$ m s^{-1}, which would suggest an upper limit of $Q^\star \sim v^2 \lesssim 10^8$ erg gm^{-1}. However, all collisions in this model are disruptive when $Q^\star < 10^6$ erg gm^{-1}, so the following will only consider the interval $10^6 < Q^\star < 10^8$ erg gm^{-1}. In the example model of Section 2.4.3, 99.7% of all collisions are destructive when $Q^\star = 10^7$ erg gm^{-1} while 89% of collisions are destructive when $Q^\star = 10^8$ erg gm^{-1}.

2.4. The Debris Disk's Time Evolution

The debris disk's dust abundance evolves due to dust production by the planetesimal rings minus losses due to collisions among dust grains. To quantify this, let $p_i = p(\beta_i, r_i)$ be the rate that one site in planetesimal ring r_i produces dust of size β_i that gets injected into streamline i. The abundance n_i of dust in streamline i then evolves according to the rate equation

$$\frac{dn_i}{dt} = p_i - \mathcal{R}_i = p_i - \frac{n_i}{T_{\text{out}}} \sum_{j=1}^{N_{r\beta}} \sum_{k=1}^{N_l} \sum_{r_1}^{r_2} \alpha_{ijk} n_j, \quad (17)$$

where the left term accounts for dust production and the right term accounts for collisional destruction, Equation (9). Index i refers to the dust that reside in the target streamline i, while j refers to dust grains in the impacting streamline j that have a relative longitude of periapse $\tilde{\omega}_k = \tilde{\omega}_j - \tilde{\omega}_i$. Although the model consists of $N_s = N_r N_l N_\beta$ streamlines, there are only $N_{r\beta} = N_r N_\beta$ equations in Equation (19) that are distinct, since the N_l streamlines that are generated in the same planetesimal ring r_i with the same dust size β_i have an identical evolution due to the system's azimuthal symmetry.

The total number of dust grains of size β_i that are generated by planetesimal ring r_i is $N_i = N_l n_i$, where N_l is the number of dust-producing sites in a planetesimal ring. Similarly, the total rate at which ring r_i produces dust of size β_i is $P_i = N_l p_i$. Multiplying Equation (17) by N_l and setting

$$\bar{\alpha}_{ij} = \frac{1}{N_l} \sum_{k=1}^{N_l} \sum_{r_1}^{r_2} \alpha_{ijk} \quad (18)$$

then provides the rate at which N_i evolves over time,

$$\frac{dN_i}{dt} = P_i - \frac{N_i}{T_{\text{out}}} \sum_{j=1}^{N_{r\beta}} \bar{\alpha}_{ij} N_j. \quad (19)$$

Here, $\bar{\alpha}_{ij}$ is the mean probability per time T_{out} that a grain of size β_i and orbit elements a_i, e_i collides with a grain of size and orbit β_j, a_j, e_j. Note that this is a mean probability since Equation (18) averages probabilities over all possible longitudes of periapse $\tilde{\omega}_k = \tilde{\omega}_j - \tilde{\omega}_i$.

This model is also going to assume that, when dust grains collide, the resulting dust fragments are so small that they are unbound and driven away by radiation pressure. This assumption simplifies the problem enormously since, if it were not true, then the number of streamlines in the debris disk would grow exponentially as collisions beget additional dusty streamlines that collide with other dust and generate even more streamlines. The validity of this assumption is confirmed later in Section 3.3.1.

2.4.1. Two-component Model

Now consider a rather simple system, that of a single planetesimal ring that manufactures dust having only two sizes, small (S) grains having radii near the blow-out radius R_{min}, and large (L) grains of radii $R_L \gg R_{\text{min}}$. In the resulting debris disk, nearly all collisions are with the small grains, due to their much greater abundance in the disk, $N_S \gg N_L$, and their much greater production rates $P_S \gg P_L$. Because small grains are only colliding with other small grains, their abundance varies as

$$\frac{dN_S}{dt} = P_S - \frac{\bar{\alpha}_{SS} N_S^2}{T_{\text{out}}} \quad (20)$$

according to Equation (19), where $\bar{\alpha}_{SS}$ is the probability density for collisions among small grains. The solution is

$$N_S(t) = N_S^{\text{eq}} \tanh(t/t_S), \quad (21)$$

where

$$N_S^{\text{eq}} = \sqrt{\frac{P_S T_{\text{out}}}{\bar{\alpha}_{SS}}} \quad \text{and} \quad t_S = \sqrt{\frac{T_{\text{out}}}{\bar{\alpha}_{SS} P_S}} = \frac{N_S^{\text{eq}}}{P_S}. \quad (22)$$

Here, N_S^{eq} is the total number of small dust grains that result when the disk settles into equilibrium, which occurs at time $t \gg t_S$ when $\tanh(t/t_S) \to 1$ and $dN_S/dt \to 0$. Note that t_S is also the small dust grains' collisional lifetime. Evidently, the small grains' equilibrium abundance as well as their optical depth will vary as $N_S^{\text{eq}} \propto P_S^{1/2}$ where P_S is their production rate, while the timescale for the disk to settle into collisional equilibrium varies as $t_S \propto P_S^{-1/2}$.

The large grains' abundance N_L also evolves according to Equation (19), which becomes $dN_L/dt = P_L - \bar{\alpha}_{LS} N_L N_S / T_{\text{out}}$ when collisions with small grains dominate. When the disk has settled into collisional equilibrium, $dN_L/dt = 0$, the equilibrium abundance of large grains is

$$N_L^{\text{eq}} = \frac{P_L T_{\text{out}}}{\bar{\alpha}_{LS} N_S^{\text{eq}}}, \quad (23)$$

where $\bar{\alpha}_{LS}$ is the large grain's collisional probability density.

Although this two-component treatment might seem too simple for quantitative work, it is illustrative, because a real disk's optical depth and collision rates are often dominated by the disk's smallest grains that have size parameters close to β_{max}. In that case, the disk's collisional equilibrium timescale and its optical depth would all vary with the square root of the planetesimal's dust-production rate. Equations (22) and (23) are also useful because they provide a convenient test of the more general debris-disk model that is developed below in Section 2.4.2; using that more general model to simulate a two-component debris yields results that agree with Equations (21)–(23) to within 0.04%.

2.4.2. Scale-Invariant Evolution

Now consider a more realistic scenario where the system's planetesimal rings produce dust whose rates are power laws in the dust size parameter β_i and planetesimal ring radius r_i such that $P_i = P_0(\beta_i/\beta_{\text{max}})^q(r_i/r_{\text{out}})^c$. It will also be convenient

to first convert Equation (19) into a dimensionless system of equations via the substitutions

$$t = T_0 t^\star \quad \text{and} \quad N_i(t) = N_0 \left(\frac{\beta_i}{\beta_{\max}}\right)^q \left(\frac{r_i}{r_{\text{out}}}\right)^c N_i^\star(t^\star), \quad (24)$$

where $t^\star = t/T_0$ is dimensionless time coordinate and $N_i^\star(t^\star) = N_i(t)P_0/P_i N_0$ is the scaled abundance of grains of size β_i produced by ring r_i. The collision probability density will also be written as $\bar{\alpha}_{ij} = (\bar{\alpha}_{ij}^\star/I)(\beta_j/\beta_{\max})^{-q}(r_j/r_{\text{out}})^{-c}(R_{\min}/r_{\text{out}})^2$ where the scaled collision probability is

$$\bar{\alpha}_{ij}^\star = \frac{1}{N_l} \sum_{k=1}^{N_l} \sum_{r_1}^{r_2} \frac{\beta_{\max}^2 f_{ijk}^c}{4 \sin \phi_{ijk}} \sqrt{\frac{1-\beta_i}{2a_j/r_{ijk}-1}} \left(\frac{\beta_i+\beta_j}{\beta_i \beta_j}\right)^2$$

$$\times \left(\frac{\beta_j}{\beta_{\max}}\right)^q \left(\frac{r_{\text{out}}^2}{r_{ijk}a_j}\right) \left(\frac{r_{\text{out}}}{a_i}\right)^{3/2} \left(\frac{r_j}{r_{\text{out}}}\right)^c. \quad (25)$$

In the above, the constant timescale T_0 and population scale-factor N_0 are

$$T_0 = \sqrt{\frac{IT_{\text{out}}}{P_0}} \left(\frac{r_{\text{out}}}{R_{\min}}\right) \quad (26a)$$

$$\text{and} \quad N_0 = P_0 T_0 = \sqrt{IP_0 T_{\text{out}}} \left(\frac{r_{\text{out}}}{R_{\min}}\right). \quad (26b)$$

Inserting this into Equation (19) then yields a system of equations

$$\frac{dN_i^\star}{dt^\star} = 1 - N_i^\star \sum_{j=1}^{N_{r\beta}} \bar{\alpha}_{ij}^\star N_j^\star \quad (27)$$

that is not just dimensionless, but also scale invariant. This is very handy, since Equation (27) need only be solved once in order to apply the result to a variety of systems that might have a range of planetesimal radii r_{out} orbiting stars of varied masses $M_\star$ and luminosities $L_\star$. Note, however, that the rescaled collision probability $\bar{\alpha}_{ij}^\star$ does depend on the dust power laws q and c, the dust grains' specific energy for collisional disruption $Q^\star$, and the planetesimal disk's radial width $r_{\text{in}}/r_{\text{out}}$ (Equation (25)), so any changes to those parameters do require solving Equation (27) again.

Equation (27) is a coupled set of nonlinear differential equations whose initial conditions are $N_i^\star(0) = 0$. These equations are easily solved numerically for each streamline's relative abundance $N_i^\star(t^\star)$ using a Runga–Kutta algorithm. That solution to Equation (27) then provides the dust grains' relative abundances $N_i(t)/N_0 = (P_i/P_0)N_i^\star(t^\star)$. A sample calculation is shown in Figure 2, which plots the relative abundances N_i/N_0 versus dimensionless time $t^\star$ for dust that is generated by a narrow planetesimal ring ($N_r = 1$ and $r_{\text{in}} = r_{\text{out}}$) whose dust production has the $q = 3.5$ size distribution that expected for debris that is in collisional equilibrium (Dohnanyi 1969). In this and all calculations that follow, the simulated debris disk is composed of grains having $N_\beta = 200$ distinct sizes, with the dust size parameters distributed over the interval $0.0652 \leqslant \beta_i \leqslant 0.497$ such that the dust grains' radii $R_i = (\beta_{\max}/\beta_i)R_{\min}$ are uniformly sampled over the interval $R_{\min} \leqslant R \leqslant R_{\max}$. Dust of each size β_i are launched from $N_l = 100$ evenly spaced longitudes about the planetesimal disk, so the resulting debris disk is comprised of $N_s = N_r N_l N_\beta = 2 \times 10^4 N_r$ distinct
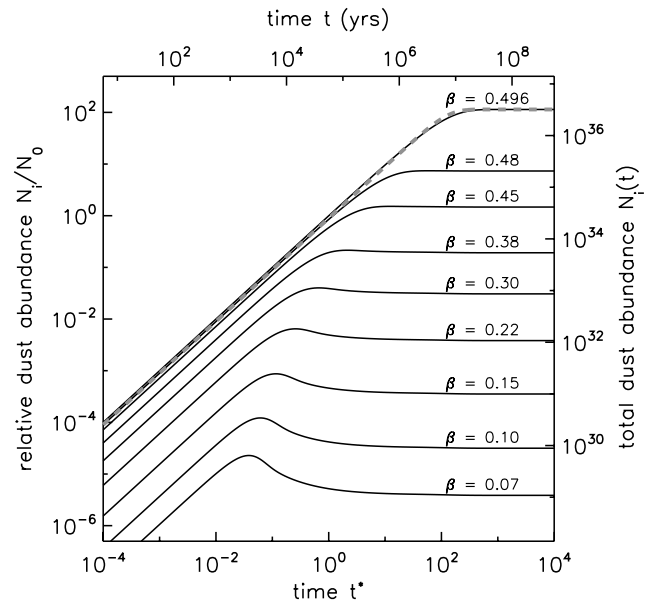
Figure 2. Equation (27) is solved for the scaled dust abundances $N_i^\star(t^\star)$ assuming that the dust is produced by a narrow planetesimal ring ($N_r = 1$) with a $q = 3.5$ size distribution. The scaled dust abundances are then converted into absolute dust abundances $N_i(t^\star)/N_0$ and plotted vs. dimensionless time $t^\star$ (left and lower axes). This model also assumed that the dust are weak, $Q^\star = 10^6$ erg gm^{-1}, so all collisions disrupt the dust. Abundances for nine selected streamlines having the indicated size parameter β are shown above; not shown are the model's 191 other curves that behave similarly. The right and upper axes are scaled for an $r_{\text{out}} = 50$ AU planetesimal ring in orbit about a solar-type star that produces dust at the rate $\dot{M}_d = 10^{13}$ gm s^{-1} with $\rho = 1$ gm cm^{-3}, $Q_{\text{rp}} = 0.96$, and $I = 0.1$ rad, for which $N_0 = 2.8 \times 10^{34}$ grains and $T_0 = 5.6 \times 10^4$ yr. The dashed gray curve is Equation (21) with an equilibrium timescale $T_{\text{eq}} = 7.1$ Myr.

streamlines. The planetesimal disk that is the source of this dust is usually composed of $N_r = 3$–5 planetesimal rings, except $N_r = 1$ is used when the dust source is a narrow planetesimal ring, as is the case for Figure 2. The β distribution used here results in streamlines that range as far as $r = 150r_{\text{out}}$ from the central star, where r_{out} is the planetesimal disk's outer radius. Execution times on a desktop PC range from 4 minutes for simulations having $N_r = 1$ to 2 hr for simulations having $N_r = 5$.

Although the calculation seen in Figure 2 covers a fairly broad range of β parameters, the resulting debris disk is nonetheless populated by dust having a fairly narrow range of sizes, since it is only the smallish dust grains that are lofted well outside of the birth ring by radiation pressure. In Figure 2, the central star is solar and the dust grains have a density $\rho = 1$ gm cm^{-3} and radiation pressure efficiency $Q_{\text{rp}} = 0.96$, so the radius of the smallest bound dust grain is $R_{\min} = 1.1$ μm, and the range of dust radii that populate the simulated debris disk is only 1.1 μm $\leqslant R \leqslant 8.5$ μm. Of course, a real disk will also manufacture larger dust, but those larger grains would be confined to the disk's innermost region $r_{\text{in}} \leqslant r \leqslant 1.15r_{\text{out}}$, so they do not alter the disk's large-scale structure at $r \gg r_{\text{out}}$. Also, these larger grains contribute little to the disk's optical depth due to their slower dust-production rates and their very short collisional lifetime, so their absence from these simulations is justified.

The parameter P_0 that appears in the constants N_0 and T_0 (Equations (26)) is related to the planetesimal disk's total dust mass production rate, which is $\dot{M}_d = \sum_i P_i \frac{4\pi}{3} \rho R_i^3$ where the sum proceeds over all streamlines that make up the dust disk. Since $P_i = P_0(\beta_i/\beta_{\max})^q(r_i/r_{\text{out}})^c$, this provides $P_0 = \dot{M}_d/S_{qc}m_{\min}$, where $m_{\min} = \frac{4\pi}{3}\rho R_{\min}^3$ is the mass

of the smallest bound dust grain, and the factor $S_{qc} = \sum_i (\beta_i/\beta_{max})^{q-3}(r_i/r_{out})^c$. Inserting this and Equation (6) into (26) then provides the scale factors

$$N_0 = \frac{2.8 \times 10^{34}}{Q_{rp}^{5/2}} \left(\frac{\dot{M}_d}{10^{13} \text{ gm s}^{-1}}\right)^{1/2} \left(\frac{I}{0.1 \text{ rad}}\right)^{1/2}$$
$$\times \left(\frac{L_\star}{L_\odot}\right)^{-5/2} \left(\frac{M_\star}{M_\odot}\right)^{9/4}$$
$$\times \left(\frac{\rho}{1 \text{ gm cm}^{-3}}\right)^2 \left(\frac{r_{out}}{50 \text{ AU}}\right)^{7/4} \left(\frac{S_{qc}}{107}\right)^{-1/2} \quad (28a)$$

and
$$T_0 = 5.6 \times 10^4 Q_{rp}^{1/2} \left(\frac{\dot{M}_d}{10^{13} \text{ gm s}^{-1}}\right)^{-1/2} \left(\frac{I}{0.1 \text{ rad}}\right)^{1/2}$$
$$\times \left(\frac{L_\star}{L_\odot}\right)^{1/2} \left(\frac{M_\star}{M_\odot}\right)^{-3/4}$$
$$\times \left(\frac{r_{out}}{50 \text{ AU}}\right)^{7/4} \left(\frac{S_{qc}}{107}\right)^{1/2} \text{ yr}, \quad (28b)$$

where the factor $S_{qc} = 107$, 320, and 530 for the simulations having $N_r = 1$, 3, and 5 planetesimal rings with $c = 0$ and $q = 3.5$. The above quantities allow one to easily rescale all figures shown here for systems having alternate dust-production rate $\dot{M}_d$ or the planetesimal disk's outer radius r_{out}, etc. The following subsection will also show that the time T_{eq} for the resulting dust disk to settle into an equilibrium where dust production balances mass loss due to collisions is $T_{eq} \simeq 130 T_0$.

2.4.3. Example: $a_r = 50$ AU Birth Ring

To illustrate, consider a narrow ($N_r = 1$) planetesimal ring of radius $r_{out} = 50$ AU in orbit about a solar-type star. This ring will have a dust mass production rate of $\dot{M}_d = 10^{13}$ gm s^{-1}, with dust having a density $\rho = 1$ gm cm^{-3} and inclinations $I = 0.1$ rad. The grains are dark, with $Q_s = 0.1$, and are asymmetric light scatters having $g = 0.4$, so the radiation pressure efficiency is $Q_{rp} = 0.96$, $N_0 = 2.8 \times 10^{34}$, and $T_0 = 5.6 \times 10^4$ yr. Multiplying the lower and left axes in Figure 2 by these constants then provides the dust abundances $N_i(t)$ versus physical time t, which can also be read off the right and upper axes of Figure 2. That figure shows that the smallest dust grains having $\beta \simeq \beta_{max}$ need the most time to settle into an equilibrium where dust production balances destruction due to collisions. The gray dashed curve in Figure 2 also shows that the abundance of the smallest dust does resembles Equation (21) when the equilibrium timescale $T_{eq} = 7.1 \times 10^6$ yr is chosen as the moment when the smallest dust have reached two-thirds their equilibrium abundance. This demonstrates that the two-component dust size model of Section 2.4.1 is in fact relevant to this kind of debris disk. And because T_0 and T_{eq} have the same dependance on the model parameters, comparison to Equation (28b) shows that $T_{eq} \simeq 130 T_0$.

After a time $t \gg T_{eq}$, the debris disk will have settled into equilibrium. The solid black curve in Figure 3 shows the disk's equilibrium grain size distribution $N(R)$, which is extracted from the rightmost part of Figure 2 and plotted versus grain radii R. That model assumes that the dust grains are weak, $Q^\star < 10^6$ erg gm^{-1}, which means that all collisions are destructive. Note that the debris disk's dust size distribution $N(R)$ is significantly steeper than the $q = 3.5$ size distribution that governs the ring's dust production (the dotted curve in
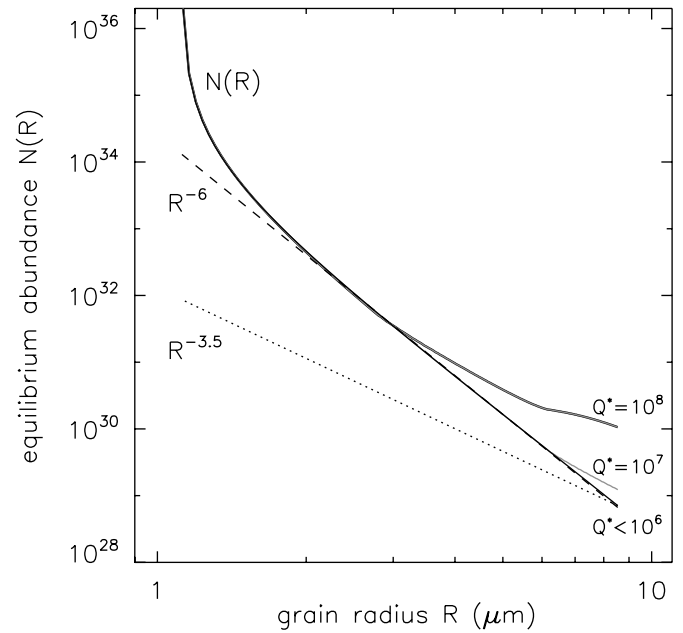

Figure 3. Black $N(R)$ curve is the differential size distribution for the dust in the debris-disk model of Figure 2 after the disk has achieved equilibrium at times $t \gg T_{eq}$ assuming the dust grains are weak with $Q^\star < 10^6$ erg gm^{-1}. Gray curves are for models having stronger dust grains, $Q^\star = 10^7$ and 10^8 erg gm^{-1}. The dashes indicate an R^{-6} size distribution, and the dotted curve is proportional to the planetesimal ring's differential dust-production rate $P(R) \propto R^{-3.5}$.

Figure 3), with $N(R) \propto R^{-6}$ except near $R \simeq R_{min}$, where it has an even steeper dependance. A peak at $R \simeq R_{min}$ is also seen in the debris-disk model[2] of Krivov et al. (2006). Figure 3 illustrates the main consequence of dust–dust collisions, which tends to destroy the disk's larger dust grains at a faster pace. However, when the dust grains are stronger, with $10^7 < Q^\star < 10^8$ erg gm^{-1}, then the larger grains are more resistant to collisional destruction, and they become more abundance (Figure 3, gray curves).

When the system is in equilibrium, the rate at which the planetesimal ring injects dust of size β_i into the debris disk, P_i, balances the rate at which collisions remove dust from the disk $\mathcal{R}_i$, so $\mathcal{R}_i = P_i$. Thus, the collisional lifetime of the grains in streamline i is $T_c(R_i) = N_i/\mathcal{R}_i = N_i/P_i$, which is plotted versus grain radius R in Figure 4 (see the black curves that are labeled by their dust-production rates $\dot{M}_d$). That lifetime is simply the time when the dust abundances $N_i(t)$ seen in Figure 2 flatten out. As expected, the smallest grains that have size parameters β that are just shy of $\beta_{max} = \frac{1}{2}$ are very long lived. This is due to their orbits having very large apoapses $Q_{apo} = r_{out}/(1-2\beta) \gg r_{out}$, so small dust spend most of their time far from the planetesimal ring, in regions where the disk's optical depth is low and collisions are rare. Note also that $T_c \propto (N_0/P_0) \propto T_0$, so the dust grains' collision timescale obeys the same scaling as Equation (28b), in particular with $T_c \propto \dot{M}_d^{-1/2}$. Figure 4 also shows that nearly all dust grains in such a debris disk have lifetimes T_c that are short compared to the age of the host star, which is typically $\sim 10^7$–10^8 yr (Meyer et al. 2007).

---

[2] Note though that the equilibrium dust size distribution in the Krivov et al. (2006) model is "wavy." Waves in a size distribution occur when some process tends to favor the rapid removal of the smallest bodies (Durda & Dermott 1997), and Figure 5 of Krivov et al. (2006) would suggest that next peak in our size distribution might occur at sizes $R \sim 1$ mm. However, these large grains would still have a very short collisional lifetime (see Figure 4), which makes their influence in the dust disk quite negligible.
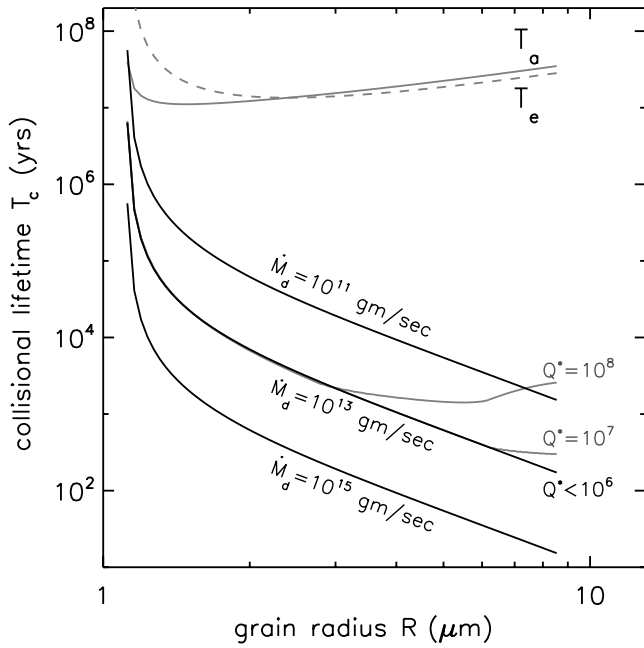
Figure 4. Lower middle black curve is the dust grain's collisional lifetime $T_c(R)$ plotted vs. dust radius R for the debris-disk model of Figure 2 that has a dust-production rate $\dot{M}_d = 10^{13}$ gm s^{-1} and strength $Q^\star < 10^6$ erg gm^{-1}, while the other black curves are for systems that are otherwise identical but with the indicated dust-production rates $\dot{M}_d$. The gray curves are for stronger dust grains having $Q^\star = 10^7$ and 10^8 erg gm^{-1} and $\dot{M}_d = 10^{13}$ gm s^{-1}; compare also to Figure 3. The upper solid gray curve T_a is the timescale over which the dust grains' semimajor decays due to PR drag, with T_e the timescale for eccentricity damping due to PR drag (see Equations (36)).

When the grains are weak, $Q^\star < 10^6$ erg gm^{-1}, then the lifetime of the larger $R \gtrsim 2R_{\min}$ varies at $T_c(R) \propto R^{-2.4}$ (Figure 4). That figure also shows that increasing the dust grains' strength $Q^\star$ increases the larger grains' longevity, without affecting the small grains' collisional lifetime. This is because all collisions are energetic enough to destroy all small grains.

2.4.4. Optical Depth

To determine the model debris disk's normal optical depth $\tau_n(r)$, it is convenient to first calculate the total dust cross section $A(r)$ that resides interior to distance r from the star. That quantity is obtained by first counting the number of dust grains $\Delta n_j(r)$ in streamline j that also lie interior r, which is $\Delta n_j(r) = \int \lambda_j d\ell$ where the integration runs along the stretch of streamline interior to r. This becomes a trivial integral over time t after noting $\lambda_j d\ell = \lambda_j v_j dt$ where $\lambda_j = n_j/v_j T_j$ is the dust grain's linear density, and n_j is the total number of grains in streamline j that have velocity v_j and orbit period T_j. Consequently, $\Delta n_j(r) = 2n_j t_j(r)/T_j$ where $t_j(r)$ is the time for dust in streamline j to travel from periapse to distance r. Since $n_i = N_i/N_l$ where N_i is the total number of dust grains in the disk that have the same sizes and orbits, the total cross section for grains of radii $R_i = (\beta_{\max}/\beta_i)R_{\min}$ that reside interior to r is $A_i(r) = N_l \Delta n_i(r)\pi R_i^2 = 2N_i(t_i/T_i)(\beta_{\max}/\beta_i)^2 \pi R_{\min}^2$. The total dust cross section interior to r is then $A(r) = \sum_i A_i(r)$ where the sum proceeds over all streamlines whose dust have distinct sizes β_i produced by planetesimal ring r_i. The ratio t_i/T_i in the above is obtained by solving $r = a_i(1 - e_i \cos E)$ for the dust grains' eccentric anomaly $E(r)$, which is then inserted into Kepler's equation to obtain $t_i/T_i = (E - e_i \sin E)/2\pi$. Also note that the differential $\Delta A = (\partial A/\partial r)\Delta r$ is the dust cross section that resides in an annulus of radius r and width Δr. Since the
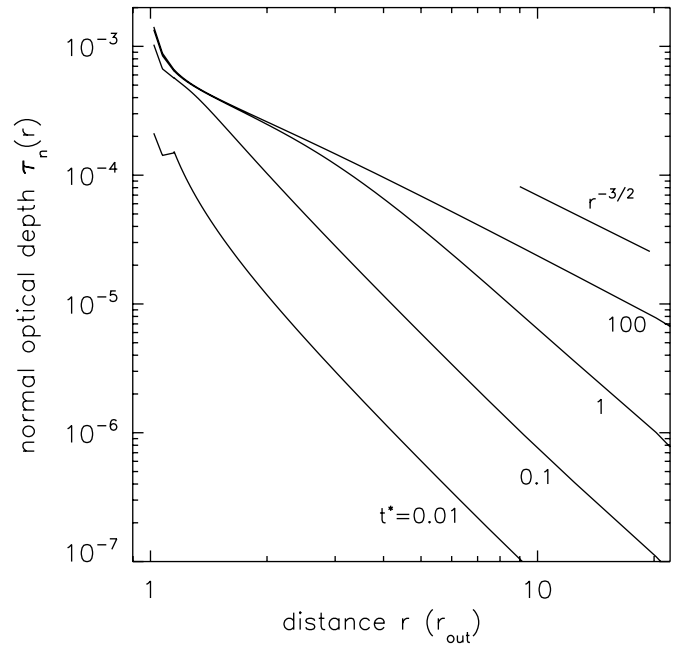
Figure 5. Dust optical depth $\tau_n(r)$ is plotted vs. distance r in units of the planetesimal disk's outer radius r_{out} for the model of Figure 2. Shown is $\tau_n(r)$ at dimensionless times $t^\star = 0.01, 0.1, 1, 100$, and an $r^{-3/2}$ curve.

disk's normal optical depth τ_n is simply the surface density of dust cross section, that quantity is

$$\tau_n(r) = \frac{\Delta A}{2\pi r \Delta r} = \frac{1}{2\pi r} \frac{\partial A}{\partial r}, \qquad (29)$$

which is easily calculated by differentiating $A(r)$ numerically.

Figure 5 plots the dust optical depth $\tau_n(r)$ versus distance r from the star at dimensionless times $t^\star = 0.01, 0.1, 1$, and 100 for the model of Figure 2. As the figure shows, it is the outer portion of the disk that is populated at later times by dust. This is due to the outer disk being composed of smaller dust that, according to Figure 2, are the last to arrive at a collisional balance. Also note that when the disk has settled into equilibrium at times $t^\star \gg 1$, the outer disk at $r \gg r_{\text{out}}$ has an optical depth $\tau_n(r) \propto r^{-3/2}$, which is in agreement with what Strubbe & Chiang (2006) call a type B debris disk.
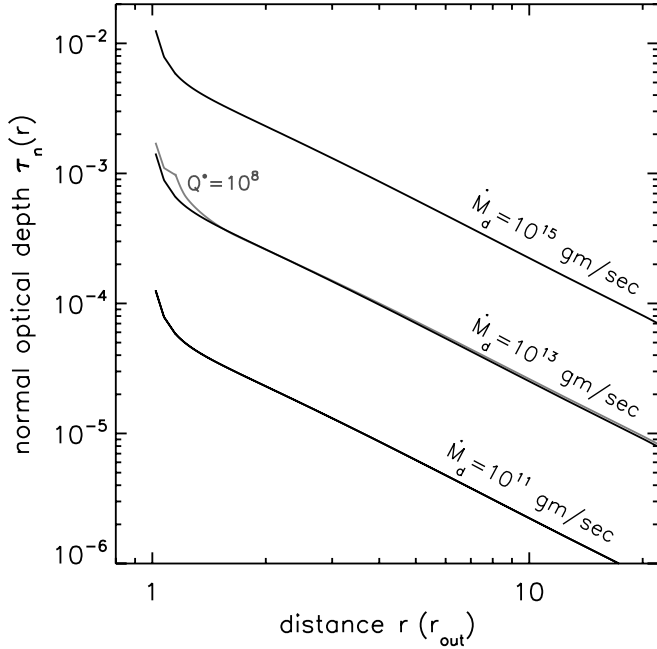
The black curves in Figure 6 show the equilibrium optical depth $\tau_n(r)$ for simulated debris disks that are identical to the one considered in Figure 2, except that different dust-production rates $\dot{M}_d$ are considered. These curves assume the dust grains are weak, with $Q^\star < 10^6$ erg gm^{-1}. As expected, these optical depths vary as $\dot{M}_d^{1/2}$ (see Equation 28a). The one gray curve there shows the optical depth of a disk composed of strong dust having $Q^\star = 10^8$ erg gm^{-1}. That disk shows a slight overdensity near the planetesimal ring, and is due to an excess of larger grains in low-eccentricity orbits (see gray curves in Figures 3 and 4).

The sharp peak in $\tau_n(r)$ at $r \simeq r_{\text{out}}$ seen in Figure 6 is due to the narrow width of the planetesimal ring that is the source of this dust. However, Figure 7 shows that peak broadens when the planetesimal ring's radial width is increased.

2.4.5. Disk Surface Brightness

This subsection will calculate the surface brightness of starlight that a simulated debris disk will scatter toward an observer that views the disk at optical wavelengths. In the following, flux F is the power per area in the incident or scattered
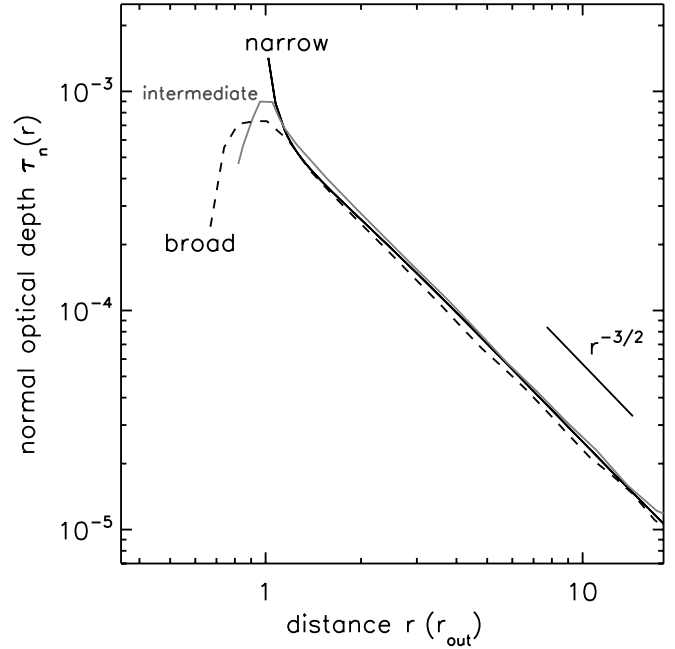
Figure 6. Black curves give the debris disk's equilibrium optical depth $\tau_n(r)$ vs. radial distance r for dust generated in a narrow debris disk of radius r_{out}. Model parameters are identical to those adopted in Figure 2 except that different dust-production rates are considered, $\dot{M}_d = 10^{11}$, 10^{13}, and 10^{15} gm s^{-1}, and weak grains having $Q^\star < 10^6$ erg gm^{-1}, while the one gray curve assumes strong dust having $Q^\star = 10^8$ erg gm^{-1}.

Figure 7. Normal optical depth $\tau_n(r)$ for three debris disks. One is generated by a narrow planetesimal ring of radius r_{out} (black curve), another by an intermediate-width planetesimal ring whose inner radius $r_{in} = 0.8r_{out}$ (gray curve), and the third due to a broad planetesimal disk having $r_{in} = 0.5r_{out}$ (dashed curve). The narrow planetesimal disk is represented by one planetesimal ring ($N_r = 1$), while the intermediate and broad disks use $N_r = 3$ and $N_r = 5$ planetesimal rings, respectively. All simulations have $c = 0$, so the dust-production rate is independent of distance r in the planetesimal disk. Model parameters are otherwise identical to those adopted in Figure 2. Also shown is an $r^{-3/2}$ curve.

radiation, intensity I is the power per solid angle in a pencil beam of radiation, and the surface brightness B is the radiation beam's power per area per solid angle.

Begin by calculating the surface brightness of a small segment of length $\delta\ell_j$ in streamline j. Summing the contributions from all such streamlines will then provide the debris disk's total surface brightness along some line of sight. Since these disks are often observed nearly edge-on, an edge-on viewing geometry is also assumed here, though these results are easily generalized for other viewing geometries as well. Segment $\delta\ell_j$ in streamline j is composed of dust having a total cross section $\delta\sigma_j$, so the intensity of starlight δI_j that is reflected by that segment is $\delta I_j = Q_s\Phi F_i \delta\sigma_j$, where $F_i = L_\star/4\pi r^2$ is the flux of incident starlight, $L_\star$ is the central star's luminosity, and r the dust grains' distance from the star. The dust grains' phase function is Φ, and it is normalized so that its integral over all solid angles is unity, with this quantity having units of steradians^{-1}. Note also that $F_i\delta\sigma$ is the power in the incident starlight while $\int \delta I_j d\Omega$ (when integrating over all solid angles $d\Omega$) is the power in the scattered light, so $Q_s = \int \delta I_j d\Omega / F_i \delta\sigma_j$ is the efficiency of light scattering by these dust grains. In planetary astronomy, this quantity is known as the Bond albedo (Lester et al. 1979).

The surface brightness of the small segment is $B_j = \delta I_j/\delta A_j$ where δA_j is the projected area on the sky occupied by that segment whose total length is $\delta\ell_j$ and projected length (as seen by the observer) is δx_j (see Figure 8). Since that segment is actually a ribbon of material of height $2Ir$ due to the dust grain's inclinations I, the segment's projected area is $\delta A_j = 2Ir\delta x_j$, and its surface brightness contribution is $B_j = (Q_s\Phi F_i/2Ir)(\delta\sigma_j/\delta x_j)$.

The number of dust grains in segment $\delta\ell_j$ is $\delta n_j = \lambda_j\delta\ell_j = \lambda_j v_j\delta t$ where v_j is the dust grains' velocity there and δt is the time for the dust to traverse $\delta\ell_j$. This becomes $\delta n_j = (n_j/T_j)\delta t$ where T_j is the dust grains' orbit period, since $\lambda_j v_j = n_j/T_j$

where n_j is the number of dust grains in streamline j that also have radius $R_j = (\beta_{max}/\beta_j)R_{min}$. Consequently, the cross section of dust in segment $\delta\ell_j$ is $\delta\sigma_j = \pi n_j(\beta_{max}/\beta_j)^2 R_{min}^2(\delta t/T_j)$. That segment has a length $\delta\ell_j = v_j\delta t$, and Figure 8 shows that its projected length is $\delta x_j = v_j|\cos(\theta + \varphi)|\delta t$ where θ is the segment's longitude as measured from the $\hat{\mathbf{x}}$-axis. The angle φ obeys $\sin\varphi = v_{j,\theta}/v_j$ and $\cos\varphi = v_{j,r}/v_j$ (see Figure 8) where $v_{j,r}$ and $v_{j,\theta}$ are the dust grain's radial and tangential velocities, Equations (13), so $\delta x_j = |v_{j,r}\cos\theta - v_{j,\theta}\sin\theta|\delta t = 2\pi a_j|\sin\theta + e_j\sin\tilde{\omega}_j|(\delta t/T_j)/\sqrt{1 - e_j^2}$. Inserting these results into B_j and noting that $n_j = N_j/N_l$ then yields $B_j = B_0\sqrt{1 - e_j^2}(\Phi\Omega_1 N_j/N_l)(R_{min}^2 r_{out}^2/r^3 a_j)(\beta_{max}/\beta_j)^2/|\sin\theta + e_j\sin\tilde{\omega}_j|$ where the constant

$$B_0 = \frac{Q_s L_\star}{16\pi I r_{out}^2 \Omega_1}. \tag{30}$$

Note that $\Omega_1 = 1$ sr is introduced into the above so that B_0 has units of surface brightness and that the combination $\Phi\Omega_1$ is dimensionless. Summing the contributions from all streamlines then yields the disk's total surface brightness $B(x) = \sum B_j$ as a function of projected distance $x = r\cos\theta$ from the central star, so

$$B(x) = B_0 \sum_{i=1}^{N_{r\beta}} \sum_{j=1}^{N_l} \sum_{\text{near}}^{\text{far}} \frac{\Phi\Omega_1 N_i\sqrt{1 - e_i^2}}{N_l|\sin\theta + e_j\sin\tilde{\omega}_j|}$$
$$\times \left(\frac{R_{min}}{r_{out}}\right)^2 \left(\frac{r_{out}^4}{r^3 a_i}\right) \left(\frac{\beta_{max}}{\beta_i}\right)^2, \tag{31}$$

where the innermost sum is over the two segments—one nearer and the other further from the observer—that intersect the
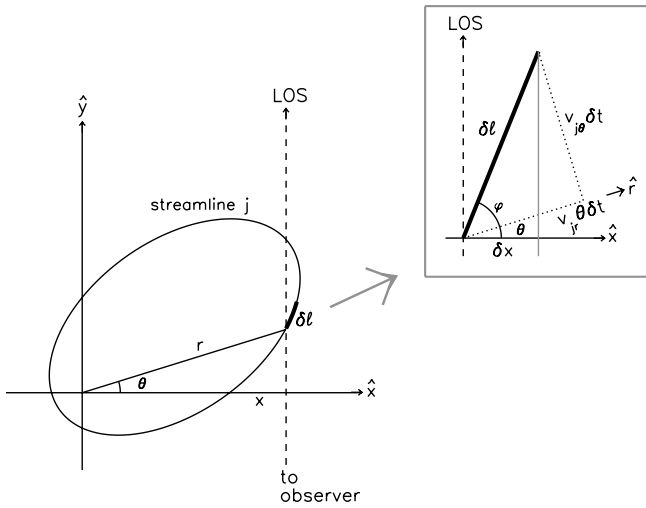
Figure 8. Observer's line of sight (LOS) passes through streamline j and intersects segment $\delta\ell$ at polar coordinates (r, θ); that segment also lies at a projected distance x from the central star at the origin. The insert zooms in on segment $\delta\ell$, which has a projected length δx when viewed by the observer. The dust in that segment will have traveled a distance $\delta\ell = v_j \delta t$ in time δt, which corresponds to radial and tangential displacements $v_{j,r}\delta t$ and $v_{j,\theta}\delta t$, so the angle φ satisfies $\sin\varphi = v_{j,\theta}/v_j$ and $\cos\varphi = v_{j,r}/v_j$. Also note that the scattering angle ϕ is the angle between the radial direction $\hat{\mathbf{r}}$ and the direction to the observer, so $\phi = \pi/2 + \theta$.

observer's line of sight (see Figure 8), while the middle sum proceeds over each streamlines' orientation $\tilde{\omega}_j$, and the leftmost sum proceeds over the $N_{r\beta}$ streamlines having distinct dust sizes β_i that originate in the various planetesimal rings r_i. Equation (31) also requires the two longitudes $\theta(x)$ where the observer's line of sight intercepts streamline j. That is obtained by solving $x = r\cos\theta$ for $\theta(x)$ where $r = p_j/[1 + e_j\cos(\theta - \tilde{\omega}_j)]$, which yields $\theta(x) = \tilde{\omega}_j - \tan^{-1}(B/A) \pm \cos^{-1}(x/\sqrt{A^2 + B^2})$ where $A = p_j\cos\tilde{\omega}_j - e_j x$, $B = p_j\sin\tilde{\omega}_j$, and $p_j = a_j(1 - e_j^2)$ is the ellipse's semilatus rectum, with the r in Equation (31) from $r = x/\cos\theta$.

The phase function employed here is the Henyey–Greenstein function

$$\Phi(\phi) = \frac{1 - g^2}{4\pi(1 + g^2 - 2g\cos\phi)^{3/2}} \quad \text{sr}^{-1} \qquad (32)$$

that is widely used in studies of circumstellar dust. The scattering angle ϕ in the above is related to the dust grain's longitude θ via $\phi = \pi/2 + \theta$ (see Figure 8). This phase function is controlled by the dust grains' asymmetry parameter $g = \int \Phi(\phi)\cos\phi\, d\Omega$ (see Equation (2)), with a positive value resulting in forward light scattering while negative values result in backscattering.

Equations (31) and (32) are used to calculate the surface brightness for three edge-on debris disks whose parameters are identical to those of Figure 2 except for differing dust-production rates $\dot{M}_d$ (see Figure 9). As expected, these surface brightness curves vary as $B \propto \sqrt{\dot{M}_d}$. Also note that $B(x) \propto x^{-7/2}$, which again is in agreement with the type B debris disk of Strubbe & Chiang (2006).

Figure 10 illustrates how the inner part of a debris disk's surface brightness depends on the degree of asymmetry in the dust grains' light scattering. For instance, when the dust grains are either isotropic light scatters ($g = 0$), or are only modestly forward scattering ($g = 0.4$), the debris disk's surface brightness profile $B(x)$ is roughly constant in the inner regions where $x \lesssim r_{\text{out}}$. However, if the light scattering by the dust
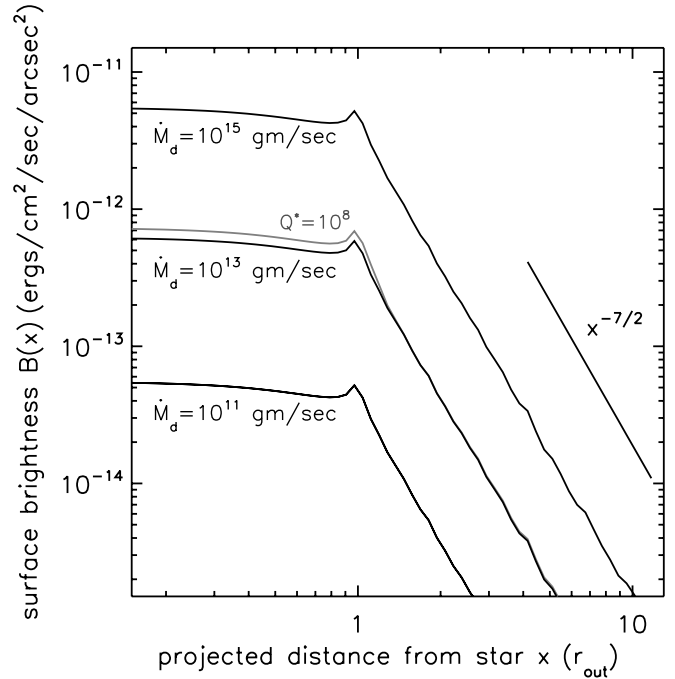

Figure 9. Equation (31) is used to calculate the surface brightness $B(x)$ vs. projected distance from the star x for three edge-on debris disks that are generated by narrow planetesimal rings that have the indicated dust-production rates $\dot{M}_d = 10^{11}$, 10^{13}, and 10^{15} gm s^{-1}. Black curves assume weak dust having $Q^\star < 10^6$ erg gm^{-1}, a light-scattering asymmetry parameter $g = 0.4$, and albedo $Q_s = 0.1$, with all system parameters identical to those of Figure 2. These curves give the disks' unfiltered surface brightnesses integrated over all optical wavelengths. An $x^{-7/2}$ curve is also shown, and the gray curve is for strong dust having $Q^\star = 10^8$ erg gm^{-1}.

is strongly asymmetric, with $g = 0.8$, then $B(x)$ continues to increase inward of $x = r_{\text{out}}$. Disks having this kind of knee bend in their surface brightness profiles appear to be common (Krist et al. 2005; Golimowski et al. 2006), with forward scattering of starlight being the preferred explanation for the bent surface brightness profile of the edge-on debris disk at AU Mic and β Pic (Strubbe & Chiang 2006; Ahmic et al. 2009). Evidently, light scattering by circumstellar dust is rather asymmetric. Lastly, note that almost identical results are obtained when the dust grains are backscattering, with $g < 0$, with those slight differences being due to the dust grains' slightly larger radiation pressure efficiency $Q_{\text{rp}} = 1 - g Q_s$. The following will assume that the grains are forward scattering, which is appropriate for dust grains that are larger than the wavelength of the incident radiation, and is consistent with forward scattering by the solar system's interplanetary dust (Lamy & Perrin 1986).

Figure 11 also shows how an edge-on disk's surface brightness $B(x)$ evolves over time. As expected, $B(x)$ gets shallower at later times as the smaller dust grains steadily populate the outer parts of the disk (see also Figures 2 and 5). Eventually, the smaller grains arrive at collisional equilibrium at dimensionless times $t^\star = t/T_0 \gg 1$, and the disk surface brightness settles into the expected $B(x) \propto x^{-3.5}$ power law. Note that at earlier times, such as at time $t^\star = 0.01$, the disk's surface brightness can be as steep as $B(x) \propto x^{-5.0}$. Consequently, disks having a surface brightness steeper than $x^{-3.5}$ might indicate that the disk is younger than time T_0, or that dust production by the planetesimal disk has increased in recent times.

Note that these surface brightness calculations assume that the dusty disk is so tenuous that the grains do not shadow each other; this assumption is confirmed in Section 3.3.2. Also
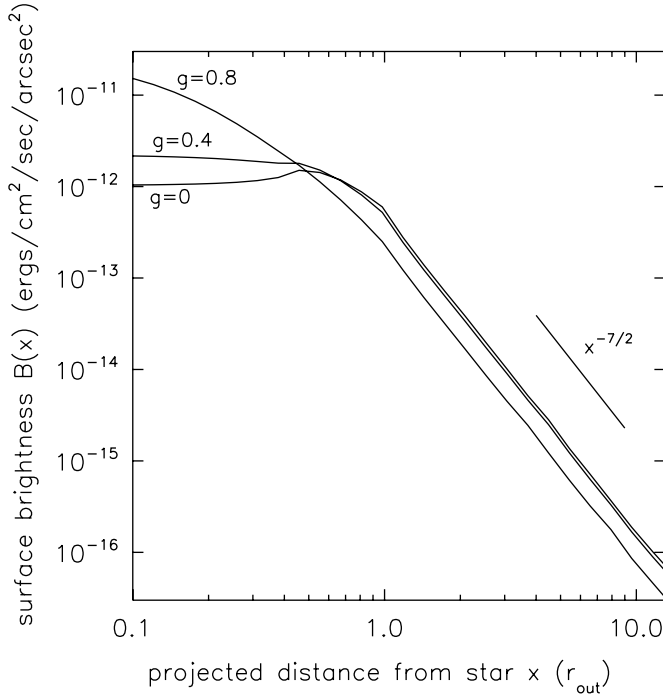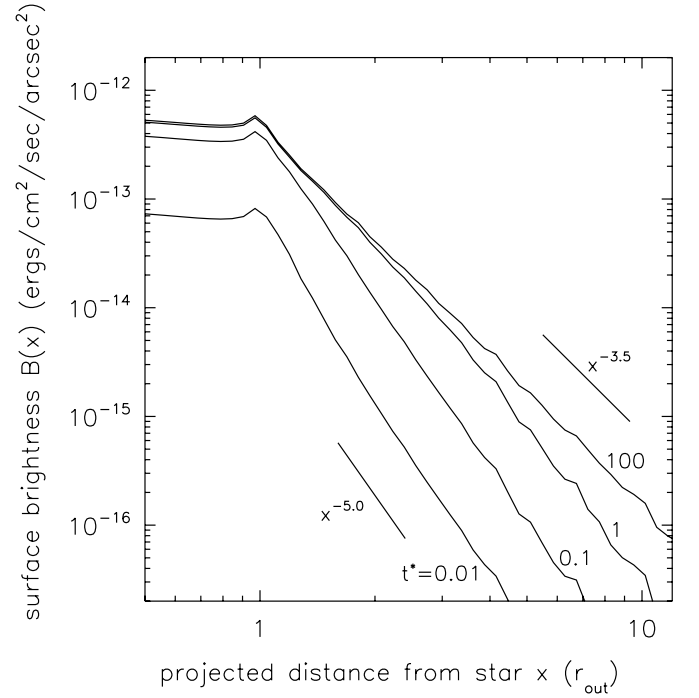
Figure 10. Surface brightness $B(x)$ is plotted vs. projected distance x for three edge-on debris disks that are generated by a broad ($r_{in} = 0.5r_{out}$) planetesimal disk having a dust-production rate $\dot{M}_d = 10^{13}$ gm s^{-1}, a light-scattering efficiency of $Q_{scat} = 0.1$, and the indicated light-scattering asymmetry parameter $g = 0, 0.4$, and 0.8. Also shown is an $x^{-7/2}$ curve. Note also that the small bump in $B(x)$ at $x = 0.5r_{out}$ (which is where the line of sight runs along the planetesimal disk's inner edge) gets washed-out when the light scattering is very asymmetric with $g \gtrsim 0.8$.

Figure 11. Surface brightness $B(x)$ is plotted vs. projected distance x (in units of r_{out}) for the debris-disk model that is described in Figures 2 and 5 viewed edge-on with $Q_s = 0.1$. Shown is $B(x)$ at dimensionless times $t^\star = t/T_0 = 0.01$, 0.1, 1, and 100, as well as power laws that vary as $x^{-3.5}$ and $x^{-5.0}$.

keep in mind that Figures 9–11 give the disks' total surface brightness integrated over all optical wavelengths. If these systems were instead observed through a narrowband filter having a central frequency ν then the star's total luminosity $L_\star = 4\pi^2 R_\star^2 \int_0^\infty B_\nu d\nu = 4\pi R_\star^2 \sigma T_\star^4$ (where $R_\star$ is the stellar radius, B_ν is the Planck function, σ the Stefan–Boltzmann constant, and $T_\star$ is the star's effective temperature) in Equation (30) should instead be replaced by its specific luminosity $\partial L_\star/\partial \nu = \pi L_\star B_\nu/\sigma T_\star^4$, so that Equations (31) and (32) would then provide the disk's surface brightness per unit frequency.

2.4.6. A Relic Debris Disk

It is also worth considering the debris disk's evolution when the planetesimal disk's dust production suddenly ceases. Such might occur if there are any planets in the system that quickly adjust their orbits, perhaps due to a rapid migration of a planet through a dense planetesimal disk (Gomes et al. 2004), or due to planet–planet scattering (i.e., the Nice model; Gomes et al. 2005). Should that occur, then the planetesimals might find themselves in unstable orbits, which then leads to a rapid dynamical erosion of the disk and a cessation of dust production.

Halting dust production is simulated here by setting the planetesimal ring's dust-production rate $P_i(t) = 0$ at all times after t_{stop}, or equivalently changing the $1 \rightarrow 0$ in the invariant evolution (Equation (27)) at dimensionless times $t^\star > t^\star_{stop}$ where $t^\star_{stop} = t_{stop}/T_0$. Solving those equations numerically shows that the larger grains in the inner part of the debris disk are quickly destroyed due to their short collisional lifetimes (Figure 4). This depletes the inner disk's optical depth and drives it toward a shallower $\tau_n(r) \propto r^{-1/2}$ power law that decreases over time. As Figure 12 shows, the cessation of dust

production also decreases the inner part of an edge-on disk's surface brightness so that $B(x) \propto x^{-5/2}$ at times $t^\star \gg t^\star_{stop}$ so the detection of a debris disk having a shallow optical depth profile $\tau_n(r) \propto r^{-1/2}$ (when the view to the disk is oblique or face-on), or an edge-on disk having a shallow $B(x) \propto x^{-5/2}$ surface brightness profile, would indicate that the object is a *relic* disk wherein dust production has ceased. That relic disk will be composed mostly of small, marginally bound grains of radii $R \simeq R_{min}$. The abundance N_S of those small dust grains will then fade over time according to Equation (20), whose solution is $N_S(t') = N_S(t_{stop})/[1 + N_S(t_{stop})\bar{\alpha}_{SS}t'/T_{out}]$ when the dust-production rate $P_S = 0$, where $t' = t - t_{stop}$ is the time since the end of dust production and $\bar{\alpha}_{SS}$ is the small grains' collisional probability density. Note that this behavior over time is typical for a system that steadily grinds away without any replenishment (cf. Wyatt et al. 2007a; Löhne et al. 2008). Inspection of the upper two curves in Figure 12 also shows that the time for the system to transform into a relic disk is about $t_{trans} \sim 10T_0 \sim 0.1T_{eq}$, i.e., the transition occurs relatively quickly in comparison to the system's equilibrium timescale T_{eq}.

3. APPLICATION TO β PICTORIS

The colored curves in Figure 13 show the surface brightness of the starlight that is scattered by the edge-on debris disk orbiting β Pictoris. These curves are extracted from images that Golimowski et al. (2006) acquired with the *Hubble Space Telescope* (*HST*) at optical wavelengths. These profiles exhibit the classic signature of a debris disk that is generated by a disk of colliding planetesimals that extends out to about $r_{out} \simeq 150$ AU, with the surface brightness falling off steeply as $B(x) \propto x^{-3.5}$ at projected distances $x \gtrsim 220$ AU, and less steep interior to r_{out}. Note also that the β Pic disk is asymmetric, with the outer part of the disk's northeast (NE, blue curve) ansa being about 50% brighter than its southwest (SW, red curve) ansa. Although
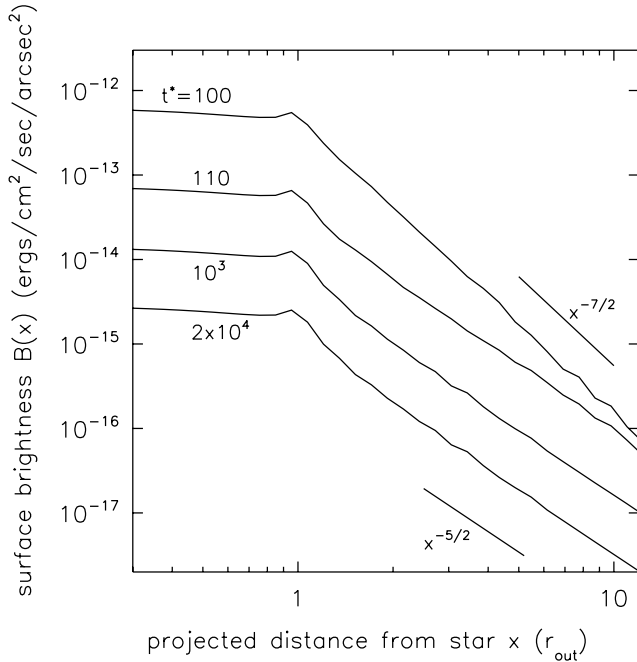
Figure 12. Dust-producing debris-disk model of Figure 2 is evolved until dimensionless time $t^\star_{stop} = 100$ when dust production ceases ($P_i = 0$). The debris disk's surface brightness $B(x)$ is shown at the indicated times $t^\star$, as well as two power laws $x^{-7/2}$ and $x^{-5/2}$.

that asymmetry is not accounted for by the axially symmetric debris-disk model that is used here, possible causes for that asymmetry are described in Section 3.3.5.

β Pic is an A5V star that lies a distance $\Delta = 19.28$ pc away, has a luminosity $L_\star = 8.7\,L_\odot$, mass $M_\star \simeq 1.8\,M_\odot$, an effective temperature $T = 8200$ K (Crifo et al. 1997), and an age of $t_\star \sim 12$ Myr (Zuckerman et al. 2001). Note that the star's peak emission occurs at wavelength $\lambda = 0.35\,\mu$m, yet the radius of the smallest bound grain is $R_{min} \simeq 3\,\mu$m assuming the grains have a density of $\rho = 1$ gm cm^{-3} and a radiation pressure efficiency $Q_{rp} = 0.53$ (Equation (6)) so this system is in the geometric optics limit, and the light-scattering theory employed here is appropriate. Figure 11 of Golimowski et al. (2006) also shows that the disk's vertical distribution has an FWHM that varies as FWHM $\propto 0.14x \sim 2h$, so the dust grains' inclinations are approximately $I = h/x \sim 0.07$ rad.

The black curve in Figure 13 shows that the debris-disk model can reproduce β Pic's observed surface brightness when the dust-producing planetesimal disk is quite broad, with inner and outer radii $r_{in} = 75$ AU and $r_{out} = 150$ AU. This system has been evolved over the star's lifetime, $t_\star = 12$ Myr, so the system is still approaching equilibrium since $T_{eq} = 20$ Myr. The dust grains must also be rather asymmetric light scatters, with $g = 0.67$ (assuming forward scattering), in order to account for the knee seen in the surface brightness profile at $x \sim 150$ AU, consistent with Ahmic et al. (2009). The model also assumes that the dust grains are rather reflective, $Q_s = 0.7$, which is the Bond albedo of Saturn's icy A and B rings at the observation wavelength (Porco et al. 2005). With these assumptions in hand, fitting the simulated surface brightness to the disk's observed $B(x)$ requires the planetesimal disk's dust-production rate to be $\dot{M}_d = 1.7 \times 10^{15}$ gm s^{-1}. The total cross section of dust in the simulated debris disk is $A_d = 1.9 \times 10^{20}$ km^2, and the total mass of dust is $M_d = 11$ lunar masses. Note that this mass is comparable to the 8 lunar masses that Holland et al. (1998) inferred from submillimeter observations of this disk, which
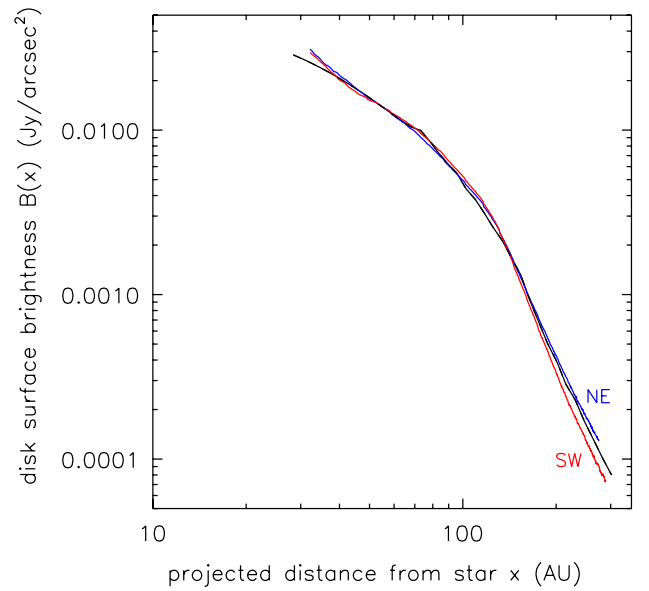

Figure 13. Red and blue curves give the surface brightness $B(x)$ of the edge-on disk orbiting β Pictoris, extracted from the *Hubble Space Telescope* observations acquired by Golimowski et al. (2006) in the F606W filter, and plotted vs. projected distance x from the central star. The black curve is for a model that adopts a $q = 2.5$ size distribution for dust produced by a broad disk of planetesimals orbiting at $75 < r < 150$ AU from the central star; this system was evolved for $t = 1.2 \times 10^7$ yr, which is the age of the central star. The simulated dust grains' inclinations are $I = 0.07$ rad = 4°0, their density is $\rho = 1$ gm cm^{-3}, and they are strong with $Q^\star = 10^8$ erg gm^{-1}. The dust grains also have a light-scattering efficiency $Q_s = 0.7$, a light-scattering asymmetry parameter $g = 0.67$, and a radiation pressure efficiency $Q_{rp} = 1 - gQ_s = 0.53$. The planetesimal disk's dust-production rate is $\dot{M}_d = 1.7 \times 10^{15}$ gm s^{-1}, so $N_0 = 3.6 \times 10^{34}$ and $T_0 = 1.5 \times 10^5$ yr, and the disk's equilibrium timescale is $T_{eq} = 2.0 \times 10^7$ yr.

supports the contention that the β Pic dust grains are rather reflective.

The dust-production rate inferred here is about $\dot{M}_d \simeq 9\,M_\oplus$ Myr^{-1}. For comparison, this rate is about 200 times higher than what Stern & Colwell (1997) report for their model of the collisional erosion of our own Kuiper Belt. Note that β Pic's dust-production rate is quite considerable, for if it has held steady over the system's lifetime, then the unseen planetesimals orbiting β Pic would have lost a total mass of $\dot{M}_d t_\star \sim 110$ Earth masses.

It should be noted that the planetesimal disk's inferred erosion rate is very sensitive to the dust grain's optical properties. Equation (31) shows that an edge-on disk's surface brightness is varies as $B \propto B_0 N_0 R_{min}^2$ where $B_0 \propto Q_s$, $N_0 \propto \dot{M}_d^{1/2}\rho^2 Q_{rp}^{-5/2}$, and $R_{min} \propto Q_{rp}/\rho$ (Equations (3), (6), (28a), and (30)), which means that the inferred dust-production rate varies as $\dot{M}_d \propto f_Q$ where $f_Q = Q_{rp}/Q_s^2$ and $Q_{rp} = 1 - gQ_s$. (Interestingly, the inferred dust-production rate is insensitive to the assumed grain density ρ, which cancels out.) If the dust grains are dark instead and have a scattering efficiency $Q_s = 0.1$, then the radiation pressure efficiency is $Q_{rp} \simeq 1$ and $f_Q \simeq 100$, which means that the dust-production rate must be ~ 100 faster if the dust grains are dark. In this case, β Pic would have lost $\sim \dot{M}_d t_\star \sim 10^4$ Earth masses over its lifetime, which is implausible. Rather, it is more likely that the dust grains at β Pic are bright.

The optical depth profile $\tau_n(r)$ that is inferred from β Pic's observed surface brightness $B(x)$ is shown in Figure 14. Note that $B(x) \propto \int Q_s \tau_n d\ell$ where the integration is along the line of sight, so the disk's optical depth is uncertain by a factor of Q_s. The $Q_s = 1$ curve obtained here is similar to the optical depth
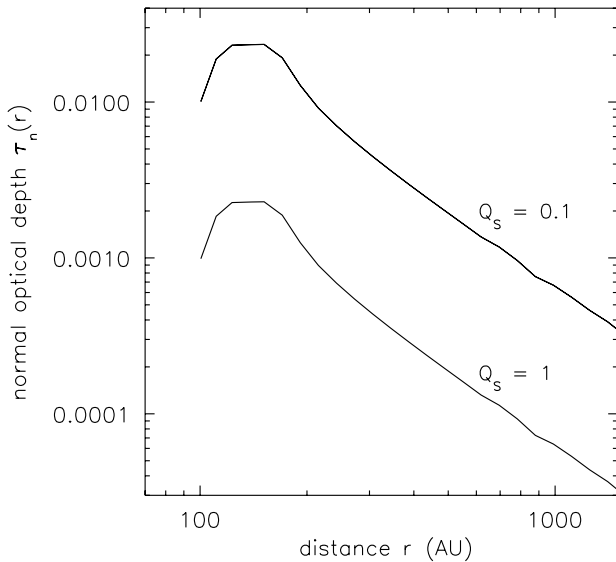
Figure 14. Normal optical depth $\tau_n(r)$ that results in the surface brightness profile shown in Figure 13, assuming $Q_s = 0.1$ and $Q_s = 1$. The dust-production rate for the $Q_s = 1$ model is 300 times smaller than the $Q_s = 0.1$ model.

profile that Ahmic et al. (2009) inferred from the same data set.[3] The range of possible values for the total dust mass M_d and total dust cross section A_d are $4.7 \leqslant M_d \leqslant 170$ lunar masses and $1.2 \times 10^{20} \leqslant A_d \leqslant 1.6 \times 10^{21}$ km^2, with the lower values for a disk composed of bright $Q_s = 1$ dust grains, and the higher values for dark $Q_s = 0.1$ dust.

3.1. Sensitivity to Parameters

The following explores the sensitivity of the above results for β Pic to the assumed model parameters.

First, the dust produced by the simulated planetesimal disk has a $q = 2.5$ size distribution, so most of the just-produced dust grains' mass is in the largest grains that actually contribute little to the debris disk's optical depth. Consequently, the dust-production rate $\dot{M}_d$ inferred above is somewhat sensitive to $\beta_{\min}$, which is the size parameter of the largest grains that are allowed in the model. The equilibrium model shown in Figure 13 has $\beta_{\min} = 0.065$ (which corresponds to a maximum grain radius $R_{\max} = 23$ μm), and it requires a dust-production rate of $\dot{M}_d = 1.7 \times 10^{15}$ gm s^{-1} when the model is fit to the disk's observed surface brightness profile assuming $Q_s = 0.7$. However, cutting off the dust size distribution at $\beta_{\min} = 0.1$ and then optimizing the other parameters then results in a fit that is only marginally acceptable; that model has $R_{\max} = 14$ μm and $\dot{M}_d = 1.2 \times 10^{15}$ gm s^{-1}. Nonetheless, models having $\beta_{\min} \gtrsim 0.2$ are ruled out, because they are deficient in grains having sizes $R > 6$ μm that would be confined to radial distances of $75 \lesssim r \lesssim 250$ AU, and their absence from the model reduces the simulated disk's surface brightness at projected distances $x \sim r$.

Interestingly, the disk's surface brightness profile $B(x)$ is rather sensitive to the size-distribution power law q. For instance, models having $q \leqslant 2.0$ do not reproduce the disk's observed surface density profile, because the model disk's inner $r \lesssim 150$ AU region is overdense with large dust grains that contribute too much surface brightness at $x \lesssim 150$ AU, while models

having $q \geqslant 3.0$ are underdense in large grains and thus too dim there. Evidently, the dust being produced by the unseen planetesimals at β Pic have a $q \simeq 2.5$ size distribution that is just a bit shallower than the canonical Dohnanyi $q = 3.5$ size distribution. And because the observed dust size distribution is constrained to $2 < q < 3$, this translates into an uncertainty in the value of $\dot{M}_d$ quoted above is no more than a factor of 2. Also, keep in mind that the value for q refers to the size distribution for dust production by the planetesimal disk, and that the debris disk's resulting dust size distribution is actually much steeper due to collisions among dust grains (e.g., Figure 3).

This kind of modeling is also sensitive to the planetesimal disk's inner and outer radii. The midpoint of the knee at $x \simeq 110$ AU in β Pic's surface brightness profile indicates that the planetesimal disk's midpoint is near $r \simeq 110$ AU (Figure 13), and best agreement with the observations is achieved when $r_{\rm in} \simeq 75$ AU and $r_{\rm out} \simeq 150$ AU, i.e., when the disk has a radial aspect ratio of $r_{\rm in}/r_{\rm out} \simeq 0.5$. However, broader disks having $r_{\rm in}/r_{\rm out} < 0.3$ are ruled out because the knee in their surface brightness profiles are too broad to fit the observations. Likewise, narrower planetesimal disks having $r_{\rm in}/r_{\rm out} \geqslant 0.8$ are ruled out because those models produce a prominent bump in the debris disk's surface brightness where $x = r_{\rm in}$, and such bumps are not seen in these optical observations. Although these surface brightness bumps are seen in infrared observations of β Pic (Wahhaj et al. 2003; Telesco et al. 2005), their locations vary with the observing wavelength, which indicates that their interpretation likely requires modeling the disk's thermal emission as well.

We have also considered "inside-out" erosion of the planetesimal disk, with $c = -2$, but the edge-on disk's surface brightness was rather similar to that generated by planetesimal disk suffering "outside-in" erosion with $c = +2$, so $c = 0$ is adopted in all models shown here. Also note that strong dust grains having $Q^\star = 10^8$ erg gm^{-1} are preferred over models that use weaker $Q^\star \leqslant 10^7$ erg gm^{-1} dust grains. The larger grain strength increases the survival of the larger dust grains (see Figure 3) that are confined to the vicinity of the planetesimal disk at $75 < r < 150$ AU. When $Q^\star \leqslant 10^7$ erg gm^{-1}, the lower abundance of large dust grains then results in a noticeable surface brightness deficit at $x \sim 100$ AU.

3.2. Implications for Planet Formation

If one adopts the plausible assumption that the β Pic dust grains are bright ($Q_s \sim 0.7$), then the mass of the planetesimal disk is likely well above 110 $M_\oplus$, which is sufficient to form about six Neptune-class planets. This planetesimal disk's considerable mass, plus its broad radial extent ($75 \lesssim r < 150$ AU), also provides several interesting constraints on the prospects for planet formation at β Pic. Analogy with the Kuiper Belt, which resides at distances $\sim$30% beyond Neptune's orbit, suggests that there should be no Neptune-class giant planets orbiting well beyond $r \gtrsim 60$ AU from β Pic, because such planets would have scattered away a portion of the inferred planetesimal disk and part of its dust disk. The fact that there are no such planets yet means that if planets are trying to form there via core accretion (e.g., a runaway accretion of planetesimals by a growing planetary embryo), then the timescale for this kind of assembly in the $75 \lesssim r < 150$ AU zone must be longer than the system's $t_\star \sim 12$ Myr age. However, gravitational instability (GI) is a much faster planet-formation mechanism, one that can also form giant planets at large stellarcentric distances (Durisen et al. 2007; Dodson-Robinson et al. 2009).

---

[3] The Ahmic et al. (2009) work does not mention Q_s; we suspect that $Q_s = 1$ was assumed there.

However, GIs are only operative when the circumstellar disk is still rich in nebula gas, and the lifetime of a gas disk is at most a few Myr. Consequently, the presence of β Pic's broad and massive planetesimal disk also tells us that planet formation via GI did not happen in the $75 \lesssim r < 150$ AU zone.

It can also be concluded that giant planets are unlikely to have formed interior to $r \sim 75$ AU and subsequently migrated or scattered deep into the $75 \lesssim r < 150$ AU zone. For if that were to have happened at β Pic, then the migrating/scattering planet would have accreted and/or scattered the planetesimal disk, causing the circumstellar dust to transition into a relic debris disk within a time $t_{\mathrm{trans}} \sim 0.1 T_{\mathrm{eq}} \sim 2$ Myr. Consequently, the probability of an astronomer observing this system before its surface brightness transitioned into a relic $B(x) \propto x^{-5/2}$ profile is $t_{\mathrm{trans}}/t_\star \sim 15\%$. This finding is also consistent with Booth et al. (2009), who show that zero of 106 stars having circumstellar dust also appear to have experienced a Nice-model scattering of giant planets.

Of course, the Nice model was not intended to explain observations of circumstellar debris disks. However, our purpose here is to show how disk observations can be used to determine whether any particular solar system scenario might also be ongoing at other circumstellar disks, or if that scenario should be regarded as a rarity among the known population of star–disk systems. Indeed, it is a curiosity that β Pic seems to be planetless at $r \gtrsim 75$ AU zone, despite having a substantial amount of planetesimal mass there. However, β Pic's heavy dust-production rate, which is at least $\dot{M}_d \sim 9 \, M_\oplus \, \mathrm{Myr}^{-1}$ (and may be much larger if the grains are darker than $Q_s = 0.7$), suggests an alternate interpretation—that the planetesimal disk orbiting β Pic is not a planet-producing disk, but is instead a planetesimal-destroying disk, due to a vigorous collisional grinding of planetesimals and a heavy mass-loss rate due to the blowout of dust by radiation pressure.

3.3. Testing the Assumptions

This subsection examines the key assumptions that are employed here. Those assumptions are (1) that collision fragments contribute little to the disk's optical depth, (2) the dusty disk is so tenuous that the dust grains are not shadowing each other, (3) that Poynting–Robertson (PR) drag is insignificant, and (4) that the planetesimal disk's dust production is steady over time. A final subsection then comments on the fact that many debris disks are non-axisymmetric.

3.3.1. Dust Fragmentation

When dust grains collide, they spawn smaller dust fragments, but their contribution to the debris disk's optical depth is ignored by this model. This is appropriate if the bulk of those fragments are sufficiently small and fast such that they are unbound and leave the system. It turns out that this assumption is quite reliable, and is confirmed from the model output. Begin with a single term in Equation (9), $\mathcal{R}_{ijk} = \alpha_{ijk} n_i n_j / T_{\mathrm{out}}$, which is the rate at which the dust in the target streamline i are destroyed due to collisions with the dust in streamline j at the site $r = r_{ijk}$ where their orbits intersect. The resulting dust fragments are presumed to have a power-law size distribution $N_f = C R_f^{-q}$, which gives the number of dust fragments of radius R_f produced by the destruction of a single target grain of radius R_i, with the coefficient C determined by mass conservation. Equations (14) and (15) then provide the speed v_f at which the fragments recoil from the collision, and their

specific energy $E = \frac{1}{2} v_f^2 - G M_\star (1 - \beta_f) / r_{ijk}$ indicates whether the collision fragments having a size parameter β_f will stay bound to the star or leave the system. The total rate at which the debris disk produces collision fragments of radius R_f is $\tilde{\mathcal{R}}_f = \sum N_f \mathcal{R}_{ijk}$ where the sum proceeds over all sites in the disk r_{ijk} where dust grains collide and produce bound fragments of radii R_f. This is the secondary dust-production rate, and it is to be compared to the planetesimal disk's dust-production rate P_f. The ratio $\tilde{\mathcal{R}}_f / P_f$ depends of the radius of the smallest possible fragment R_s. Also recall that R_{min} is the radius of the smallest bound dust grain that is produced in the planetesimal disk, so $R_s < R_{\mathrm{min}}$. In this instance, the above algorithm finds that $\tilde{\mathcal{R}}_f \ll P_f$, which means that the rate at which collision are injecting second-generation dust fragments into the debris disk is negligible in comparison to the rate at which the planetesimal disk is injecting first-generation dust into the disk. For example, when $R_s < 0.5 R_{\mathrm{min}}$, this algorithm finds that $\tilde{\mathcal{R}}_f / P_f < 1\%$ when applied to the example model of Section 2.4.3. The ratio $\tilde{\mathcal{R}}_f / P_f$ is small because most of the collision fragments are small, unbound, and do not contribute to the debris disk, which justifies the model's neglect of dust fragmentation.

3.3.2. Shadowing

If the disk is sufficiently dense, then dust grains can shadow each other and alter the disk's surface brightness profile $B(x)$. The calculations presented above all assumed that the dust grains are not shadowing each other, and that assumption is confirmed by examining the disk's radial optical depth τ_r (Weidenschilling 2010). Begin with a narrow annulus in the disk of radius r and radial width Δr. The cross section of dust in that annulus is $\Delta A = \tau_n(r) 2\pi r \Delta r$ where $\tau_n(r)$ is the disk's normal optical depth. The annulus' vertical thickness is $2Ir$, so its optical depth along a radial line of sight is $\Delta \tau_r = \Delta A / 2\pi r 2 Ir = \tau_n \Delta r / 2 Ir$. The total radial optical depth of dust interior to r is then

$$\tau_r(r) = \int_0^r \frac{\tau_n(r') dr'}{2 Ir'}, \qquad (33)$$

which is easily integrated numerically. When this quantity is not small, then the dust grains at r are shadowed by interior dust, which reduces the stellar illumination there by a factor $e^{-\tau_r}$. But if $\tau_r \ll 1$ then the dust grains are fully illuminated.

Most of the debris-disk models described in the previous sections have $\tau_r < 10^{-3}$. The two exceptions are the heavy dust-producing models, such as those having $\dot{M}_d = 10^{15}$ gm s^{-1} that have $\tau_r \sim 0.01$ (Figures 4, 6, and 9), while the β Pic model that considers dark $Q_s = 0.1$ dust grains has $\tau_r \sim 0.04$. So in summary, shadowing by dust grains is not significant for the debris-disk models considered here.

3.3.3. Poynting–Robertson Drag

PR drag is a weak force that causes the orbits of small dust grains to slowly decay. The following shows that this orbital decay is negligible for the dust in the β Pic debris disk.

PR drag is the acceleration that results when a moving grain absorbs and/or scatters stellar photons. Because a grain's motion also results in a slight "headwind" of photons, the transfer of momentum, from the photons to the grain, causes its orbit to decay. The acceleration on a dust grain due to PR drag is (Burns et al. 1979)

$$\mathbf{a}_{\mathrm{PR}} = -\frac{\beta G M_\star}{r^2} \left(\frac{2 v_r}{c} \hat{\mathbf{r}} + \frac{v_\theta}{c} \hat{\boldsymbol{\theta}} \right), \qquad (34)$$

where v_r and v_θ are the grain's radial and tangential velocities (Equations (13)) and $\hat{\mathbf{r}}$, $\hat{\boldsymbol{\theta}}$ are unit vectors in a polar coordinate system. Inserting this into the Lagrange planetary equations and time-averaging those equations over an orbit then provides the rates at which an orbiting dust grain's semimajor axis a and eccentricity e decay due to PR drag,

$$\dot{a} = -\frac{2\beta G M_\star}{ac}\frac{1 + \frac{3}{2}e^2}{(1 - e^2)^{3/2}} \tag{35a}$$

$$\text{and} \quad \dot{e} = -\frac{5\beta G M_\star e}{2\sqrt{1 - e^2}a^2 c} \tag{35b}$$

(Wyatt & Whipple 1950; Burns et al. 1979). The timescales associated with this orbit decay are

$$T_a = \frac{a}{|\dot{a}|} = \frac{(1 - e^2)^{3/2}}{\beta\left(1 + \frac{3}{2}e^2\right)}\left(\frac{a}{r_{\text{out}}}\right)^2 T_{\text{PR}} \tag{36a}$$

$$\text{and} \quad T_e = \frac{e}{|\dot{e}|} = \frac{4\sqrt{1 - e^2}}{5\beta}\left(\frac{a}{r_{\text{out}}}\right)^2 T_{\text{PR}}, \tag{36b}$$

where the constant

$$T_{\text{PR}} = \frac{r_{\text{out}}^2 c}{2G M_\star} = 2.0 \times 10^6 \left(\frac{M_\star}{M_\odot}\right)^{-1}\left(\frac{r_{\text{out}}}{50\ \text{AU}}\right)^2 \text{ yr.} \tag{37}$$

Inserting Equations (5) and (7) into the above shows that these timescales are simple functions of grain size β or R. If these orbit decay timescales are long compared to a dust grains' collisional lifetime T_c, then it is appropriate to ignore PR drag.

These orbit decay timescales are plotted in Figure 4 for the example debris disk that is generated by a planetesimal ring of radius $r_{\text{out}} = 50$ AU (see Sections 2.4.3 –2.4.5 and Figures 2–11). All of these curves diverge for small grains that have radii $R \simeq R_{\text{min}}$ and size parameters $\beta \simeq \frac{1}{2}$. Note that for most grain sizes $T_c(R) \ll T_a(R)$, which means that the effects of PR drag are negligible over the lifetime of grains that are only slightly larger than R_{min}. Figure 4 also shows that PR drag is only significant when the system's dust-production rate $\dot{M}_d$ is sufficiently low, which can make $T_c \gtrsim T_a$ large, but only for these small $R \simeq R_{\text{min}}$ grains. But this only occurs when $\dot{M}_d \lesssim 10^{11}$ gm s^{-1}, for the scenario considered in Figure 4. A similar result was obtained by Wyatt (2005), who showed that PR drag is only significant when the debris disk is sufficiently tenuous. Finally, note that PR drag is completely negligible ($T_c \ll T_a$) for grains of all sizes in the β Pic debris disk, due to its very vigorous dust-production rate and the grains' short collisional lifetimes.

3.3.4. Dust Production Over Time

The model employed here assumes that the planetesimal disk's dust-production rate is steady over time, but this assumption might seem debatable, because the collisional erosion that drives dust production will ultimately decrease the planetesimal disk's mass over time. However, keep in mind that accretion within the planetesimal disk tends to produce larger bodies whose gravity can stir-up the planetesimal disk, and that can instead increase the disk's dust-production rate. Further, simulations of the collisional/accretional evolution of a planetesimal disk show that the outcomes are very sensitive to the planetesimal disk's initial conditions that are poorly known (Weidenschilling 2010). Due to this uncertainty, and that any rigorous

treatment of the planetesimal disk's evolution goes well beyond the intended scope of this study, this model makes the simplest possible assumption, that the planetesimal disk's dust-production rate is steady over time. This assumption is also justified by the collisional evolution models of Stern & Colwell (1997) and Kenyon (2002), who obtain a slow erosion timescale of ∼500 Myr for a Kuiper Belt orbiting at $r \sim 40$ AU. Because the timescale over which the erosion rate varies is likely longer than β Pic's equilibrium timescale ($T_{\text{eq}} \sim 20$ Myr, Section 3), the debris disk is expected to remain in quasi-static equilibrium as it adjusts to any slow change in the dust-production rate. Consequently, the debris-disk mass and dust-production rate inferred here are expected to be reliable.

Also note that β Pic's dust-production rate is considerable, at least $\dot{M}_d \sim 9\ M_\oplus$ Myr^{-1}. Consequently, steady dust production over the age of the system $t_\star$ also requires a large reservoir of planetesimal mass M_p, with $M_p \gg \dot{M}_d t_\star \sim 110\ M_\oplus$, i.e., the mass in β Pic's Kuiper Belt at $75 \lesssim r \lesssim 150$ AU must be well in excess of 110 Earth masses. Alternatively, if β Pic's Kuiper Belt does not satisfy $M_p \gg 110\ M_\oplus$, then collisions among planetesimals plus blowout by radiation pressure are going to grind down this extra-solar Kuiper Belt in a few×$t_\star \sim$ tens of Myr. In this case, the assumption of steady dust production does not hold, but it does mean that dust production was probably more vigorous in the past. Regardless, β Pic's planetesimal disk is or was very massive.

3.3.5. Disk Asymmetry

Many edge-on debris disks are lopsided, with one ansa substantially brighter than the other; examples include β Pic (Heap et al. 2000), AU Mic (Krist et al. 2005), and HD 15115 (Kalas et al. 2007). It may be that circumstellar debris disks are routinely non-axisymmetric. Once possible explanation for a disk's asymmetry is a recent dust-producing collision in the planetesimal disk. Recall that the orbits of all the dust grains produced in a single collision have their longitudes of periapse $\tilde{\omega}$ aligned (Section 2.1). Because dust produced in a collision tend to loiter at their apoapse, the debris disk will have an excess of dust at longitudes $\theta = \tilde{\omega} + \pi$. So if that collision was vigorous enough to produce a substantial amount of dust, then the disk will be non-axisymmetric, and may appear lopsided when viewed edge-on.

Another possible explanation for a disk's asymmetry is described in Hahn (2009), who showed that if the circumstellar dust is produced by an eccentric planetesimal ring, then the smaller dust grains produced at the ring's periapse are less bound to the star due to their higher orbital velocities there. Consequently, there will be fewer small and marginally bound grains in the direction of the ring's apoapse, which will make that part of the debris disk dimmer than the periapse side that also has an excess of small grains. This is a particularly interesting scenario since it also implies that an extra-solar planet is likely present in order to maintain the planetesimal ring's forced eccentricity.

Both of these scenarios will be explored in a follow-up study using a more advanced version of the debris-disk model that will be generalized to handle the collisional evolution of a non-axisymmetric debris disk.

Lastly, it should be noted that this model also ignores the planetesimals' free eccentricity e_f that is associated with the random part of their noncircular motions. Equations (13) and (14) in Thébault et al. (2003) show that the planetesimals' random motions tend to blur the simple relationship between a dust

grain's orbit and its size parameter (e.g., Equations (5) and (7)). However, this effect will be small when the planetesimals eccentricity e_f is small, which in fact is a requirement in order for planetesimals to have formed in the first place.

4. SUMMARY AND CONCLUSIONS

A numerical model for a circumstellar debris disk is developed and applied to observations of β Pictoris. The model accounts for dust production by colliding planetesimals and dust destruction due to collisions among grains. These rates for dust production and collisional destruction also provide a rate equation whose solution gives the dust abundance over time and as a function of grain size. That solution also provides the debris disk's grain size distribution, which is steepened substantially by collisions among dust grains. These calculations also give the dust grains' collisional lifetime $T_c(R)$, which depends on the planetesimal disk's dust-production rate $\dot{M}_d$ and grain radius R.

Scaling laws are derived, and it is shown that the dust abundance N in the debris disk varies as $N \propto \dot{M}_d^{1/2}$ once the disk has settled into collisional equilibrium, and that dust lifetimes vary as $T_c \propto \dot{M}_d^{-1/2}$. It is also shown that the radial drift of dust grains due to PR drag is unimportant provided the dust-production rate is sufficiently high so that the grains' collisional lifetimes are short compared to the drift timescale. The model also recovers the results of Strubbe & Chiang (2006), who showed that the debris disk's optical depth varies as $\tau_n(r) \propto r^{-3/2}$ when in equilibrium, and that an edge-on disk's surface brightness varies as $B(x) \propto x^{-7/2}$, where r and x are the radial and projected distances from the central star. Note though that those optical depth and surface brightness profiles will be steeper if the disk is young and not yet in collisional equilibrium. Alternatively, those profiles will be shallower if dust production has ceased in the past, which might occur if planets form in (or migrate or scatter into) the planetesimal disk and cause its dynamical depletion.

It is also shown that these quantities are not very sensitive to the dust grains' strength $Q^\star$ when $Q^\star < 10^8$ erg gm^{-1}. However, an edge-on disk's surface brightness profile is quite sensitive to the dust grain's light-scattering asymmetry parameter g, and disks like the ones at β Pic and AU Mic having a "knee" in their surface brightness indicates that the dust are very asymmetric light scatters, with $|g| \gtrsim 0.7$.

The model's principal dynamical parameters are the planetesimal disk's radius and its dust-production rate, so a comparison to observations then yields estimates of or else limits on these important cosmogonic quantities. For instance, fitting the model to optical *HST* observations of β Pic shows good agreement with the disk's observed surface brightness profile when the unseen dust-producing planetesimal disk there is quite broad, extending over $75 \lesssim r \lesssim 150$ AU. This disk's dust-production rate is also quite heavy, $\dot{M}_d \sim 9\ M_\oplus$ Myr^{-1}, if it is assumed that the dust grains are bright like Saturn's rings ($Q_s = 0.7$). In this case, the total cross section of dust in the debris disk is $A_d = 1.9 \times 10^{20}$ km^2, and the inferred mass there is $M_d = 11$ lunar masses. Note that this mass is comparable to that previously inferred from submillimeter observations of this disk (Holland et al. 1998). Also, it is unlikely that the dust grains at β Pic are dark (i.e., with $Q_s < 0.1$), since that would require the planetesimal disk to grind away at a rate that is implausible. Indeed, the mass-loss rates inferred here are so heavy as to

suggest that the $r \gtrsim 75$ AU zone at β Pic might be a region of planetesimal destruction due to collisional grinding, rather than a site of ongoing planet formation.

The model developed here is called ddisk, which is an easy-to-use IDL script that others might wish to use as they diagnose their observations of circumstellar debris disks. This code is available for download at http://gemelli.spacescience.org/∼hahnjm/software.html.

REFERENCES

Ahmic, M., Croll, B., & Artymowicz, P. 2009, ApJ, 705, 529
Booth, M., Wyatt, M. C., Morbidelli, A., Moro-Martín, A., & Levison, H. F. 2009, MNRAS, 399, 385
Burns, J. A., Lamy, P. L., & Soter, S. 1979, Icarus, 40, 1
Crifo, F., Vidal-Madjar, A., Lallement, R., Ferlet, R., & Gerbaldi, M. 1997, A&A, 320, L29
Dodson-Robinson, S. E., Veras, D., Ford, E. B., & Beichman, C. A. 2009, ApJ, 707, 79
Dohnanyi, J. W. 1969, J. Geophys. Res., 74, 2531
Durda, D. D., & Dermott, S. F. 1997, Icarus, 130, 140
Durisen, R. H., Boss, A. P., Mayer, L., Nelson, A. F., Quinn, T., & Rice, W. K. M. 2007, Protostars and Planets V, ed. B. Reipurth, D. Jewitt, & K. Keil (Tucson, AZ: Univ. Arizona Press), 607
Golimowski, D. A., et al. 2006, AJ, 131, 3109
Gomes, R., Levison, H. F., Tsiganis, K., & Morbidelli, A. 2005, Nature, 435, 466
Gomes, R. S., Morbidelli, A., & Levison, H. F. 2004, Icarus, 170, 492
Hahn, J. M. 2009, in 40th Annual Meeting, AAS, Division of Dynamical Astronomy (Washington, DC: AAS), 06.12
Heap, S. R., Lindler, D. J., Lanz, T. M., Cornett, R. H., Hubeny, I., Maran, S. P., & Woodgate, B. 2000, ApJ, 539, 435
Holland, W. S., et al. 1998, Nature, 392, 788
Holsapple, K., Giblin, I., Housen, K., Nakamura, A., & Ryan, E. 2002, Asteroids III, 443
Holsapple, K. A. 1994, Planet. Space Sci., 42, 1067
Kalas, P., Fitzgerald, M. P., & Graham, J. R. 2007, ApJ, 661, L85
Kenyon, S. J. 2002, PASP, 114, 265
Krist, J. E., et al. 2005, AJ, 129, 1008
Krivov, A. V., Löhne, T., & Sremčević, M. 2006, A&A, 455, 509
Lamy, P. L., & Perrin, J. 1986, A&A, 163, 269
Lester, T. P., McCall, M. L., & Tatum, J. B. 1979, J. R. Astron. Soc. Canada, 73, 233
Levison, H. F., Morbidelli, A., Vanlaerhoven, C., Gomes, R., & Tsiganis, K. 2008, Icarus, 196, 258
Löhne, T., Krivov, A. V., & Rodmann, J. 2008, ApJ, 673, 1123
Meyer, M. R., Backman, D. E., Weinberger, A. J., & Wyatt, M. C. 2007, in Protostars and Planets V, ed. B. Reipurth, D. Jewitt, & K. Keil (Tucson, AZ: Univ. Arizona Press), 573
Porco, C. C., et al. 2005, Science, 307, 1226
Stern, S. A., & Colwell, J. E. 1997, ApJ, 490, 879
Strubbe, L. E., & Chiang, E. I. 2006, ApJ, 648, 652
Telesco, C. M., et al. 2005, Nature, 433, 133
Thébault, P., Augereau, J. C., & Beust, H. 2003, A&A, 408, 775
Wahhaj, Z., Koerner, D. W., Ressler, M. E., Werner, M. W., Backman, D. E., & Sargent, A. I. 2003, ApJ, 584, L27
Weidenschilling, S. J. 2010, ApJ, submitted
Wyatt, M. C. 2005, A&A, 433, 1007
Wyatt, M. C., Smith, R., Greaves, J. S., Beichman, C. A., Bryden, G., & Lisse, C. M. 2007a, ApJ, 658, 569
Wyatt, M. C., Smith, R., Su, K. Y. L., Rieke, G. H., Greaves, J. S., Beichman, C. A., & Bryden, G. 2007b, ApJ, 663, 365
Wyatt, S. P., & Whipple, F. L. 1950, ApJ, 111, 134
Zuckerman, B., Song, I., Bessell, M. S., & Webb, R. A. 2001, ApJ, 562, L87